

EMBRY-RIDDLE

Aeronautical University™

SCHOLARLY COMMONS

Dissertations and Theses

12-2013

Robust Image-Based Visual Servo Control of an Uncertain Missile Airframe

Murat Tunca Aygun

Embry-Riddle Aeronautical University - Daytona Beach

Follow this and additional works at: <https://commons.erau.edu/edt>



Part of the [Aerospace Engineering Commons](#)

Scholarly Commons Citation

Aygun, Murat Tunca, "Robust Image-Based Visual Servo Control of an Uncertain Missile Airframe" (2013). *Dissertations and Theses*. 18.

<https://commons.erau.edu/edt/18>

This Thesis - Open Access is brought to you for free and open access by Scholarly Commons. It has been accepted for inclusion in Dissertations and Theses by an authorized administrator of Scholarly Commons. For more information, please contact commons@erau.edu.

Robust Image-Based Visual Servo Control of an Uncertain Missile Airframe

by

Murat Tunca Aygun

A thesis submitted to the

Physical Sciences Department

in partial fulfilment of the requirements for the degree of

Master of Science in Engineering Physics

Embry-Riddle Aeronautical University

Daytona Beach, Florida

December 2013

© Murat Tunca Aygun

December 2013

Robust Image-Based Servo Control of an
Uncertain Missile Airframe

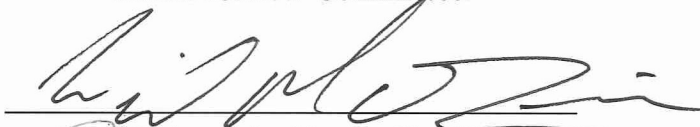
by

Murat Tunca Aygun

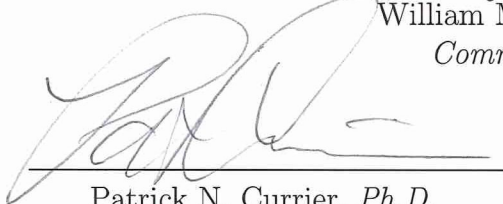
This thesis was prepared under the direction of the candidate's thesis committee chair, Dr. William MacKunis, Department of Physical Sciences, and has been approved by the members of the thesis committee. It was submitted to the Department of Physical Sciences and was accepted in partial fulfillment of the requirement of the Degree of

Masters of Science in Engineering Physics

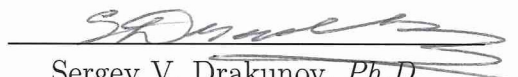
Thesis Review Committee:



William MacKunis, *Ph.D.*
Committee Chair



Patrick N. Currier, *Ph.D.*
Committee Member



Sergey V. Drakunov, *Ph.D.*
Committee Member



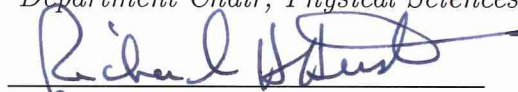
Peter Erdman, *Ph.D.*
MSEP Graduate Program Coordinator



Terry Oswalt, *Ph.D.*
Department Chair, Physical Sciences



William Grams, *Ph.D.*
Dean, College of Arts & Sciences



for Robert Oxley, *Ph.D.*
Associate Vice President of Academics

12/18/2013

Date

THIS PAGE INTENTIONALLY LEFT BLANK

Abstract

A nonlinear vision-based guidance law is presented for a missile-target scenario in the presence of model uncertainty and unknown target evasive maneuvers. To ease the readability of this thesis, detailed explanations of any relevant mathematical tools are provided, including stability definitions, the procedure of Lyapunov-based stability analysis, sliding mode control fundamentals, basics on visual servo control, and other basic nonlinear control tools. To develop the vision-based guidance law, projective geometric relationships are utilized to combine the image kinematics with the missile dynamics in an *integrated visual dynamic system*. The guidance law is designed using an image-based visual servo control method in conjunction with a sliding-mode control strategy, which is shown to achieve asymptotic target interception in the presence of the aforementioned uncertainties. A Lyapunov-based stability analysis is presented to prove the theoretical result, and numerical simulation results are provided to demonstrate the performance of the proposed robust controller for both stationary and non-stationary targets.

THIS PAGE INTENTIONALLY LEFT BLANK

Acknowledgements

Foremost, I would like to express my deepest gratitude to my advisor, Dr. William MacKunis, for his enthusiasm, support, patience, and motivation during my studies.

I would like to thank my thesis committee members, Dr. Patrick Currier, Dr. Sergey Drakunov, and Dr. Mahmut Reyhanoglu for their insightful and constructive comments which I believe will serve as the foundation for my continuing research.

Special thanks also to Embry-Riddle Aeronautical University which made this study possible.

I would like to express my appreciation to all friends and peers. Their continuous support provided me with much needed humor and motivation.

Finally, and most importantly, I would like to thank my family, Ahmet S. & Guler Saner for providing me the opportunity to a better education and a bright future. I am deeply grateful for their tremendous support, encouragement, and patience throughout my education. I dedicate this paper to the Saner family to signify their sacrifice, devotion and faith in me.

THIS PAGE INTENTIONALLY LEFT BLANK

Contents

Signature	3
Acknowledgements	7
List of Figures	11
1 Introduction	13
2 Background	20
2.1 Nonlinear System Stability	20
2.1.1 Basic Stability Calculations	26
2.1.2 Existence and Uniqueness of Solutions	27
2.1.3 Stabilization of Nonlinear Systems Using Linearization	29
2.2 Robust Control	31
2.2.1 Nonlinear Damping	32
2.2.2 Sliding Mode Control	34
2.2.2.1 Existence of a Sliding Mode	36
2.3 Visual Servo Control	38
2.3.1 The Basics of Visual Servoing	39

2.3.2	Position-Based Visual Servo Control	41
2.3.3	Image-Based Visual Servo Control	43
2.3.3.1	The Interaction Matrix	43
3	Dynamic and Kinematic Models	46
3.1	Coordinate Frames	46
3.1.1	Missile Frame	46
3.1.2	Earth-Fixed Frame	46
3.1.3	Reference Frame	47
3.1.4	Camera Frame	47
3.2	Missile Dynamics	49
3.2.1	Linear Acceleration	49
3.2.2	Angular Acceleration	51
3.2.3	Equation of Motion	52
3.3	Image Kinematics	53
4	Control System	59
4.1	Control Objective	59
4.2	Control Development	59
5	Stability Analysis	63
6	Simulation - Stationary Target	66
7	Simulation - Non-Stationary Target	72
8	Conclusion	77

List of Figures

2.1	Stable Equilibrium Point	21
2.2	Unstable Equilibrium Point	21
2.3	Lyapunov Stability	23
2.4	Local Asymptotic Stability	24
2.5	Global Asymptotic Stability	25
2.6	Instability	26
2.7	Sliding Mode Control	35
2.8	Chattering	36
2.9	Homography	42
2.10	Projection Model	44
3.1	Coordinate Frames	48
3.2	Camera and Missile Frames	55
3.3	Projection Model	56
3.4	Actual vs. Virtual Camera Frames	58
6.1	Tracking and Error Minimization - Stationary Target	68
6.2	Linear and Angular Velocities - Stationary Target	69

6.3	Control Inputs - Stationary Target	70
6.4	3D Interception - Stationary Target	71
7.1	Tracking and Error Minimization - Nonstationary Target	73
7.2	Linear and Angular Velocities - Nonstationary Target	74
7.3	Control Inputs - Nonstationary Target	75
7.4	3D Interception - Nonstationary Target	76

Chapter 1

Introduction

Nonlinear differential equations are used to model dynamical systems in engineering. There are many well-established design and analysis techniques for linear time-invariant (LTI) systems; however, one or more parts of a dynamic system model may not be linear. Most real life systems contain complex nonlinearities, which render linear control methods insufficient [Wie, 1998; Khalil, 2002; Nise, 2007]. Nonlinear differential equations cannot be analytically solved, which creates challenges in control design for nonlinear dynamic systems. Lyapunov stability analysis is a popular method for analyzing the stability and convergence properties of nonlinear systems without explicitly solving the governing differential equations. Lyapunov-based stability analysis is deeply rooted and well proven in the controls community [Khalil, 2002]. Since mathematical models of dynamic systems are never perfect, parametric uncertainties and unknown disturbances must be considered for control design. To address this challenge, adaptive and robust control methods can be used in conjunction with Lyapunov-based techniques to achieve reliable and accurate control of

nonlinear systems with ill-defined or uncertain dynamic models.

Although real-world systems are often nonlinear in general, linear approximation of these systems can sometimes be satisfactory for dynamic system modelling and control system design. Analysis of linear systems can be simplified since the corresponding dynamic equations can be solved analytically. Based on this convenient fact, the stability properties of linear systems can be analyzed in a straightforward manner. In addition, there exists a set of conditions that can be used to determine the controllability and observability of a LTI system. However, as stated earlier, linear approximation of nonlinear systems is valid only under certain conditions when the system is in the vicinity of an equilibrium point. In many situations, the system motion might not remain sufficiently close to an equilibrium point. In addition, linearization often discards inherent system nonlinearities such as saturation, switching, and friction, for example, which can lead to dynamic models that are not accurately defined. Nonlinear control theory studies the application of rigorous mathematical methods to control design for systems that cannot be suitably analyzed using linear design techniques. Nonlinear control methods have the capability of achieving reliable control over a wide range of operating conditions, making nonlinear control systems suitable for a wide range of applications [Utkin, 1977; Hornik et al., 1989; Slotine et al., 1991; Papanikolopoulos et al., 1991, 1993; Lewis, 1996; Young et al., 1996; Qu, 1998; Deguchi, 1998; Wie, 1998; Hagan and Demuth, 1999; Wang and Stengel, 2000; Khalil, 2002; Zak, 2003; Xu et al., 2004; Chwa et al., 2004; Patre et al., 2006; Hamel and Mahony, 2007; Yanushevsky, 2007; Mehta et al., 2011, 2012b, a; Mackunis et al., 2007; Dupree et al., 2007; Dixon, 2007; Hu et al., 2009; Wilcox et al., 2009; Zaeim et al., 2010; Tahri et al., 2010; Cheah et al., 2010;

Mebarki et al., 2010; Zong et al., 2011; Copot et al., 2012; Zhubing et al., 2012]. To develop controllers for nonlinear systems containing significant model uncertainty, commonly used control methods employ neural network-based approaches [Hornik et al., 1989; Lewis, 1996; McFarland and Calise, 1997; Hagan and Demuth, 1999; Patre et al., 2008; McFarland and Calise, 2000; Han and Balakrishnan, 2002; Miljković et al., 2012], adaptive control methods [McFarland and Calise, 1997, 2000; Han and Balakrishnan, 2002; Miyasato, 2003; Zak, 2003; Dixon, 2007; MacKunis et al., 2010b; Cheah et al., 2010; Mehta et al., 2011, 2012a], and robust control techniques [Slotine et al., 1991; Qu, 1998; Wang and Stengel, 2000; Zak, 2003; Wilcox et al., 2009; MacKunis et al., 2010a; Zhubing et al., 2012].

The uncertainties and complex nonlinearities inherent in vision-based systems necessitate the development of advanced nonlinear control methods. Challenges in visual servo control design include dynamic model uncertainty, camera calibration errors, and pixel noise. Visual servo control (VSC) is the process of using vision-based feedback measurements to control a dynamic system. The information-rich nature of vision-based data has made VSC an attractive option in various industrial, medical, military, and robotic applications [Hutchinson et al., 1996; Malis et al., 1999; Corke and Hutchinson, 2001; Chaumette and Hutchinson, 2006; Chaumette et al., 2007; Slotine et al., 1991; Papanikolopoulos et al., 1991; Yanushevsky, 2007; Mackunis et al., 2007; Dupree et al., 2007; Hu et al., 2009; Mebarki et al., 2010; Mehta et al., 2012b, a]. Although theoretical VSC design has been widely investigated in literature [Hutchinson et al., 1996; Chaumette and Hutchinson, 2006; Chaumette et al., 2007], implementation of VSC systems was limited until recent decades due to limitations on available computational power and electronic equipment. With modern electronic capabilities,

active/passive vision systems have become a more viable option [Kim et al., 2002; Seetharaman et al., 2006; Langelaan, 2007]. Vision-based missile guidance is one popular application of VSC.

As presented by Waldmann [2002], the vision-based missile interception problem is often considered in terms of missile-to-target kinematics, or line-of-sight kinematics, which neglect the missile dynamics about the center of gravity. Corke and Good [1996] showed that an accurate representation of the missile system is necessary in high performance visual servo control to ensure dynamically realizable closed-loop controller performance. Accurate representation of a missile dynamic model is a challenge task, however, since it involves quantities that might be difficult to obtain (e.g., inertia, aerodynamic friction, external disturbances).

Intelligent and adaptive control methods are popularly utilized to compensate for system uncertainty. Neural-network (NN)-based controllers exploit the universal approximation property of NNs to compensate for system uncertainty through an offline learning (training) process. A linearly parameterized feedforward NN controller is developed by McFarland and Calise [1997] for a bank-to-turn missile to estimate/predict the uncertainties present in the dynamic system. Miljković et al. [2012], present a switching NN controller to support the vision-based control of a robotic manipulator using a reinforcement learning technique. They showed that the NN controller was capable of choosing the optimal course of action despite camera calibration errors, modelling errors, and image noise existing in the system. In some cases, NN-based techniques are combined with other control methods to improve overall system performance [McFarland and Calise, 1997; Patre et al., 2008]. For example, Patre et al. developed an asymptotic tracking controller for uncertain dynamic systems by aug-

menting a multilayer NN with a robust nonlinear feedback control element in 2008. Although NN-based control methods have been shown to perform well in their respective tasks, such methods can require increased computational power, which might not be available in certain applications.

Adaptive control methods are a popular alternative to NN-based techniques for control of systems containing uncertainty. While NNs *learn* about the dynamic system through offline training, adaptive controllers can compensate for parametric uncertainty in real time using online adaptive parameter update laws. Unlike NN controllers, adaptive methods handle uncertainties without the necessity to train offline, making them a more practical control method for some applications [Zak, 2003; Dixon, 2007; MacKunis et al., 2010b; Mehta et al., 2012a]. Mehta et al. [2012a, b] have developed an adaptive guidance law for a vision-based missile that achieves near zero miss distance interception of a target undergoing unknown evasive maneuvers.

While adaptive and NN-based control methods can compensate for system uncertainty, both methods can burden the system with a heavy computational load. Robust control methods, on the other hand, can compensate for unknown disturbances, model uncertainties and nonlinearities without the need for online adaptation of offline training.

SMC systems appeared as a subset of variable structure control (VSC) in the 1950s at the Institute of Control Sciences, in Moscow, and Moscow University, USSR [DeCarlo et al., 2000]. SMC has been shown to be capable of compensating for model uncertainty, unknown disturbances, and nonlinearities without the need for parameter adaptation, state estimation, or linearization [Qu, 1998]. The simplistic approach and robustness of VSC and SMC systems have resulted in successful utilization in

a wide range of applications such as autonomous systems, industrial and military technologies and spacecraft systems [Slotine et al., 1991; Byun et al., 1991, 1992; Drakunov, 1993; Drakunov and Utkin, 1995; Drakunov et al., 1995; Grossimon et al., 1996; Moon et al., 2001; Zak, 2003].

VSC and SMC designs involve defining a so-called switching surface (or sliding surface) at which the controller changes - often instantaneously - its structure based on the position and velocity of the system's state trajectory, causing the state to converge a desired state trajectory. It can be shown that asymptotic (zero steady-state error) convergence of the state to a desired state trajectory can be achieved through instantaneous switching between structures. This instantaneous switching is a characteristic of SMC, and it enables SMC to be extremely robust with respect to rapidly changing uncertainty in dynamic systems. SMC's robustness can be used to address control challenges including underactuation, unmodelled nonlinearities, and external disturbances, which may be present in a dynamic system. The requirement of instantaneous switching in SMC has is a concern from an application standpoint, since no physical actuators can change instantaneously. This instantaneous switching about the sliding surface can result in the undesirable "chattering" phenomenon, which will be described in detail in the SMC section. However, it should be noted that the capabilities of modern digital electronics can make digital SMC implementation a more viable option through accurate approximation of the instantaneous switching.

To eliminate the need for infinite bandwidth that is inherent in SMC, techniques such as higher-order SMC, integral SMC, equivalent control methods, and others have been proposed [Drakunov, 1992; Wang and Stengel, 2000; Patre et al., 2008; Wilcox et al., 2009; MacKunis et al., 2010a; Zhubing et al., 2012].

The robust integral of the signum of the error (RISE) control technique employs an integral signum term that can compensate for smooth bounded disturbances [Qu, 1998]. The RISE controller structure eliminates the infinite bandwidth requirement that exists in standard SMC. Integral SMC methods like RISE have been shown to yield asymptotic tracking in the presence of disturbance and model uncertainty [Patre et al., 2008].

In 1996, Drakunov et al. proposed the design of an observer using the equivalent control method to obtain additional information from the system. This approach approximates equivalent values of the discontinuous signum function in sliding mode to address problems that arise in SMC due to its discontinuous nature.

A nonlinear vision-based guidance law is presented in this paper for a missile-target scenario in the presence of model uncertainty and unknown target evasive maneuvers. To this end, projective geometric relationships are utilized to combine the image kinematics with the missile dynamics in an *integrated visual dynamic system*. The guidance law is designed using an image-based visual servo control method in conjunction with a sliding-mode control strategy, which is shown to achieve asymptotic target interception in the presence of the aforementioned uncertainties. To ease readability of this thesis, background on nonlinear control and vision-based methods are provided. A Lyapunov-based stability analysis is presented to prove the theoretical result, and numerical simulation results are provided to demonstrate the performance of the proposed robust missile guidance law for both stationary and non-stationary targets.

Chapter 2

Background

2.1 Nonlinear System Stability

Stability theory is an inseparable part of control system design and analysis. There are various kinds of stability problems that appear in the study of dynamical systems. We are interested in the stability of equilibrium points. The foundation for the study of the stability of equilibrium points was laid by the Russian mathematician and engineer, Aleksandr Lyapunov, in his book *The General Problem of Stability of Motion* in 1892. For control purposes, equilibrium points are classified as stable or unstable. An equilibrium point, x^* , is considered to be **stable** if all solutions (i.e., trajectories) starting within some finite neighbourhood of the point remain within a finite neighbourhood of the point; otherwise, the equilibrium point is **unstable**. The system is **asymptotically stable** if, in addition to being stable, solutions also converge precisely to the equilibrium point x^* as time approaches to infinity. An example of a stable equilibrium point can be seen in Figure (2.1), where, in the

absence of friction, a perturbation causes a pendulum to oscillate indefinitely within some finite neighborhood of the equilibrium point. If in addition there is friction, the pendulum will be asymptotically stable and converge to the equilibrium point. An example of an unstable equilibrium point can be seen in Figure (2.2). In this case, if there is a small perturbation, the pendulum will never return to the equilibrium point.

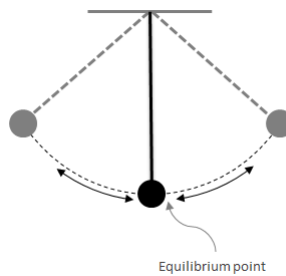


Figure 2.1: Stable Equilibrium Point

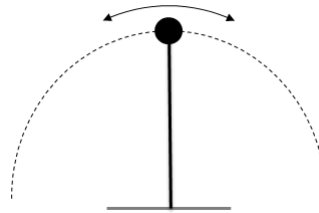


Figure 2.2: Unstable Equilibrium Point

The mathematical theorems developed by Lyapunov are indispensable tools for analyzing the stability properties of nonlinear systems for which explicit solutions are not possible to obtain. There are two primary stability theorems proposed

by Lyapunov. Lyapunov's first stability theorem, also known as Lyapunov's indirect method, uses system linearization near an equilibrium point to analyze the local stability properties of the corresponding nonlinear system. Lyapunov's second stability theorem, or Lyapunov's direct method, uses a function (i.e., Lyapunov function) analogous to a potential function to evaluate nonlinear system stability without linearizing or solving the differential equation of the system. These stability theorems will be described in detail in the following sections.

Consider a nonlinear dynamic system described by

$$\dot{x} = f(x, t) \tag{2.1}$$

where $f : [0, \infty] \times \mathcal{D} \rightarrow \mathbb{R}^n$ is a locally Lipschitz map from domain $D \subset \mathbb{R}^n$ into \mathbb{R}^n , and $x = \{x_1, x_2, \dots, x_n\}$ is a vector containing state parameters. A point $x^* \in D$ is an equilibrium point for the dynamic system defined above provided

$$f(x^*, t) = 0 \quad \forall t \tag{2.2}$$

In other words, if the state of the system is at an equilibrium point x^* , it remains at that equilibrium point for all time t .

The definitions of stability are categorized as follows.

- **Lyapunov Stability** An isolated equilibrium point x^* of the dynamic system described by (2.1), is said to be *Lyapunov stable*, or just *stable*, if for any $\epsilon > 0$ there exists a real positive number $\delta(\epsilon, t_0)$ such that

$$\|x(0) - x^*\| \leq \delta \longrightarrow \|x(t)\| < \epsilon \tag{2.3}$$

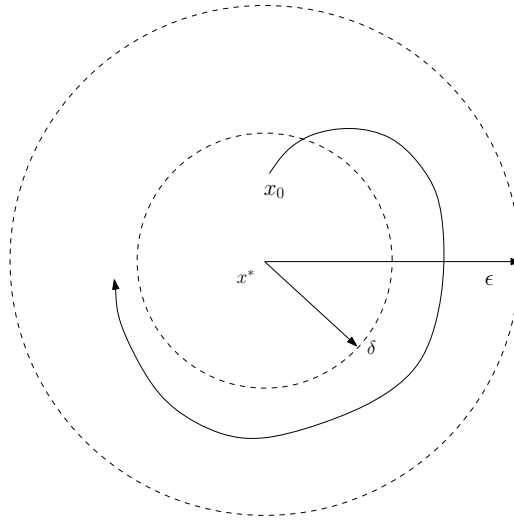


Figure 2.3: Lyapunov Stability: The system starting at x_0 stays in the vicinity of the equilibrium point x^* .

- **Local Asymptotic Stability**

An isolated equilibrium point x^* is said to be *locally asymptotically stable*, or simply *asymptotically stable*, if it is Lyapunov stable and

$$\|x(0) - x^*\| \leq \delta \implies x(t) \rightarrow x^* \quad \text{as } t \rightarrow \infty \quad (2.4)$$

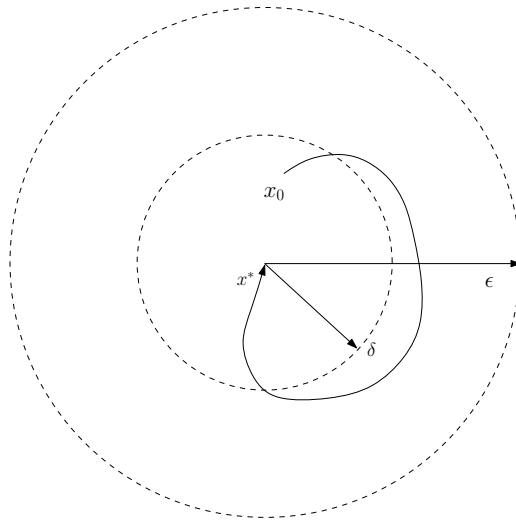


Figure 2.4: Local Asymptotic Stability: State trajectories starting at x_0 in some finite neighborhood of the equilibrium point x^* converge to the equilibrium point x^* .

- **Global Asymptotic Stability** An isolated equilibrium point x^* is said to be *globally asymptotically stable* if it is Lyapunov stable and $x(t) \rightarrow x^*$ as $t \rightarrow \infty$ for **any** initial condition $x(t_0)$.

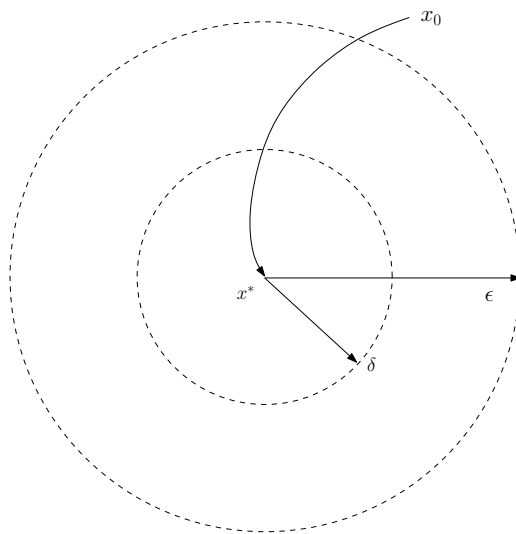


Figure 2.5: Global Asymptotic Stability: The system starting at *any* initial point x_0 converges to the equilibrium point x^* .

- **Instability** An equilibrium point is said to be *unstable* if it is neither Lyapunov stable nor asymptotically stable.

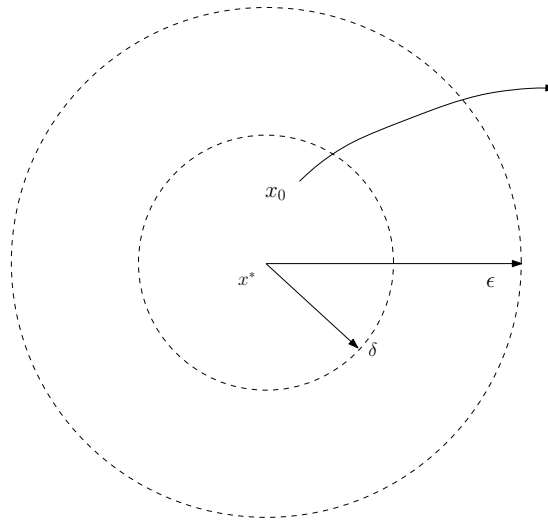


Figure 2.6: Instability: If the system is not stable, state trajectories initially displaced from the equilibrium point x^* will never converge to the equilibrium point x^* .

Note 1

- It is necessary that an equilibrium point be isolated for it to be locally asymptotically stable.
- It is necessary that an equilibrium point be the **only** equilibrium point for it to be globally asymptotically stable.

2.1.1 Basic Stability Calculations

Consider the LTI system

$$\dot{x}(t) = Ax(t) + Bu(t) \tag{2.5}$$

where $x(t) \in \mathbb{R}^n$, $A \in \mathbb{R}^{n \times n}$, $B \in \mathbb{R}^{n \times n}$, and $u(t) \in \mathbb{R}^n$. The control input $u(t)$ can be designed based on the full-state feedback law

$$u(t) = -Kx(t) \tag{2.6}$$

where $K \in \mathbb{R}^{n \times n}$ is a user-defined control gain matrix. Note that, for simplicity, it was assumed that the number of control inputs in $u(t)$ equals the number of states in $x(t)$; a simple extension can be shown to address the case where there are more control inputs than states, and the scenario where there are more states than control inputs (i.e., an underactuated system) is not being addressed here. After substituting (2.6) into (2.5) and reorganizing, the closed-loop system is obtained as

$$\dot{x} = (A - BK)x \tag{2.7}$$

The stability of the origin of the dynamic system (2.5) is determined by the eigenvalues of $(A - BK)$ from (2.7). The solution to the linear differential equation (2.7) is

$$x(t) = e^{(A-BK)t}x_0 \tag{2.8}$$

It is then obvious that for the state $x(t)$ to go to zero as $t \rightarrow \infty$, the real parts of the eigenvalues of $(A - BK)$ must be negative.

2.1.2 Existence and Uniqueness of Solutions

The existence and uniqueness of solutions to ODEs are important for the state equation $\dot{x} = f(x, t)$ to be a useful mathematical model of a dynamic system. The existence and uniqueness can be guaranteed by applying some constraints on $f(x, t)$.

Consider the initial value problem (IVP)

$$\dot{x} = f(x, t), \quad x(t_0) = x_0 \quad (2.9)$$

A continuous function $x(t)$ is considered a solution of (2.9) over an interval $[t_0, t_1]$ if $\dot{x}(t)$ is defined, and $\dot{x} = f(x, t)$ for all $t \in [t_0, t_1]$. The solution $x(t)$ will be continuously differentiable if $f(x, t)$ is continuous in both x and t .

In order to include the time-varying step changes of input, it will be assumed that $f(x, t)$ is continuous in x , but only piecewise continuous in t . In such a case, the solution $x(t)$ can only be piecewise continuously differentiable.

A function is piecewise continuously differentiable if it is continuously differentiable throughout the subdomain where it is continuous in t ; the function may not be differentiable at the points between these subdomains.

The IVP given in (2.9) may have several solutions for a given initial condition (IC). Continuity of $f(x, t)$ and its arguments guarantees that there is at least one solution; however, this is not sufficient to guarantee the uniqueness of the solution. The following theorem uses the Lipschitz condition to prove existence and uniqueness of solutions to (2.9).

Theorem 1 *If $f(x, t)$ is a piecewise continuous function in t and satisfies the Lipschitz condition,*

$$\|f(x, t) - f(y, t)\| \leq \mathcal{L}\|x - y\|$$

$\forall x, y \in B = \{x \in R^n \mid \|x - x_0\| \leq \rho\}$ for all $t \in [t_0, t_0 + \delta]$ then there exists some $\delta > 0$ such that the IVP defined in (2.9) has a unique solution over $[t_0, t_0 + \delta]$ [Khalil, 2002].

2.1.3 Stabilization of Nonlinear Systems Using Linearization

In this section, the local stability properties of an equilibrium point of a nonlinear system will be analyzed by first linearizing the system about the equilibrium point in question. It will then be shown how information about the stability properties of the linearized system can be used to determine the stability properties of the nonlinear system in a finite neighborhood of the equilibrium point.

Consider a nonautonomous system

$$\dot{x} = f(x, t) \tag{2.10}$$

where $x \in \mathcal{D}$, $f : [0, \infty] \times \mathcal{D} \rightarrow \mathbb{R}^n$ is locally Lipschitz and piecewise continuous, and $\mathcal{D} \subset \mathbb{R}^n$ is a domain that contains the origin. To linearize the system about the equilibrium point, the following transformation is introduced:

$$z = x - x^* \tag{2.11}$$

where $z(t)$ represents a deviation from the equilibrium point x^* , which is used to obtain

$$\dot{x} = \dot{z} = f(x^* + z, t) \tag{2.12}$$

After linearization, (2.12) can be written as:

$$\dot{z} = \mathbf{A}z \tag{2.13}$$

where A is a constant Jacobian matrix evaluated at x^* .

The origin $z = 0$ of the linearized system (2.13) is asymptotically stable if all the eigenvalues of \mathbf{A} have negative real parts. It is Lyapunov stable if none of the eigenvalues has a positive real part, and if there are no repeated eigenvalues on the imaginary axis. The stability properties of the linearized system (2.13) can be used to determine the stability properties of the equilibrium point x^* of the nonlinear system within a finite neighborhood of the equilibrium point.

Theorem 2 *Lyapunov's First Stability Theorem*

- If the origin $z = 0$ of the linearized system is asymptotically stable, then the equilibrium point x^* of the nonlinear system is locally asymptotically stable.
- If the origin $z = 0$ of the linearized system is unstable, then the equilibrium point x^* of the nonlinear system is also unstable.
- If the origin $z = 0$ of the linearized system is Lyapunov stable, then nothing can be said about the equilibrium point x^* of the nonlinear system based on linear analysis.

Theorem 3 *Lyapunov's Second Stability Theorem*

Lyapunov's first stability theorem analyzes the local convergence properties of a solution. Lyapunov's second stability theorem makes use of a function $V(x)$, which is analogous to a potential function, to analyze the stability of the nonlinear system based on the following conditions.

If there exists in some finite neighborhood D of the equilibrium point x^* , a positive definite scalar function $V(x)$ with continuous first partial derivative with respect to x and t satisfying the conditions

- $V(x) > 0$ for all $x \neq x^*$ in D , $V(x^*) = 0$ for all t .
- $\dot{V}(x) \leq 0$ for all $x \neq x^*$ in D and t , then the equilibrium point x^* is *Lyapunov stable*.

If in addition:

- $\dot{V}(x)$ is not identically zero along any solution x of the dynamic system other than x^* , then the equilibrium point x^* is *locally asymptotically stable*.

If in addition:

- There exists in entire state space, a positive definite function $V(x)$ which is radially unbounded (i.e., $V(x) \rightarrow \infty$ as $\|x\| \rightarrow \infty$), then the equilibrium point x^* is *globally asymptotically stable*. (i.e., $x(t) \rightarrow x^*$ as $t \rightarrow \infty$ for **any** initial condition $x(t_0)$)
- $\dot{V}(x) > 0$ for all $x \neq x^*$ and t , and $\dot{V}(x^*) = 0$ for all t , then the system is *unstable*.

2.2 Robust Control

The theory of robust control has been an active area of research in dealing with uncertainty since the late 1970s. Robust control methods are designed to achieve robust performance and/or stability in the presence of bounded modelling errors.

Unlike adaptive methods, robust controllers do not adapt to measurement variations, but rather remain static during operation assuming that certain unknown variations will be bounded. Therefore robust controllers tend to be designed based on the worst case scenario for uncertainty.

Sliding mode control, a branch of robust control, which is used in the controller design in this dissertation will be explained in this section.

2.2.1 Nonlinear Damping

Consider the following dynamical system.

$$\dot{x} = f(x, t) + u(t) \quad (2.14)$$

where $x(t) \in R$ is the state, $u(t) \in R$ is the control input, and $f(x, t)$ is an unknown disturbance that is bounded and continuous such that the following inequalities hold:

$$|f(x, t)| \leq \zeta, \quad |\dot{f}(x, t)| \leq \zeta_0, \quad |\ddot{f}(x, t)| \leq \zeta_1 \quad \forall x \in R \quad \text{and} \quad \forall t \geq 0 \quad (2.15)$$

where $\zeta, \zeta_0, \zeta_1 \in R^+$ are known constants. The control input is designed in order to minimize the ultimate magnitude of $x(t)$ as

$$u = -(k_s + 1)x \quad (2.16)$$

where $k_s \in R^+$ is a constant nonlinear damping gain. The closed-loop dynamics can be written as

$$\dot{x} = f(x, t) - (k_s + 1)x \quad (2.17)$$

In order to analyse the stability of the dynamic system, we define a Lyapunov function as

$$V = \frac{1}{2}x^2 \quad (2.18)$$

The time derivative of the Lyapunov function along trajectories of the closed-loop system can be obtained as

$$\dot{V}(x) = xf(x, t) - (k_s + 1)x^2 \quad (2.19)$$

The time derivative of the Lyapunov function is then upper bounded as

$$\dot{V}(x) \leq -x^2 - k_s(|x|^2 - \frac{\zeta}{k_s}|x|) \quad (2.20)$$

where the inequalities in (2.15) were used. After completing the squares, the bounding inequality can be expressed as

$$\dot{V}(x) \leq -x^2 + \frac{\zeta^2}{4k_s} \leq -2V + \frac{\zeta^2}{4k_s} \quad (2.21)$$

The system is concluded to be *globally uniformly ultimately bounded* [Corless and Leitmann, 1981]. Specifically, $\dot{V}(x)$ is negative outside the residual set

$$S = \{x \mid |x| \leq \frac{\zeta}{2\sqrt{k_s}}\} \quad (2.22)$$

This analysis can be used to conclude that $x(t)$ is bounded and converges to the compact set S . Therefore, the robust feedback control design is capable of achieving bounded convergence of the states, where the size of the residual set S can be made arbitrarily small by increasing the control gain k_s .

The nonlinear damping controller introduced is continuous, therefore the closed loop dynamics can be shown to have a unique solution. The solution is shown to exponentially converge to a residual set that is a function of the disturbance and can be made arbitrarily small (but not zero). A disadvantage of the nonlinear damping is that k_s is required to be large in order reduce the residual error.

2.2.2 Sliding Mode Control

Unlike the continuous nonlinear damping-based control method, sliding-mode control (SMC) uses a discontinuous control signal that can be shown to yield asymptotic convergence of the state to the origin or to a desired state.

Depending on the systems position in state-space, the controller switches from one continuous structure to another, driving it toward the adjacent region in every cycle. This will lead the system to slide along the boundaries of the control structures. The motion of the system sliding along these boundaries is called the "sliding mode".

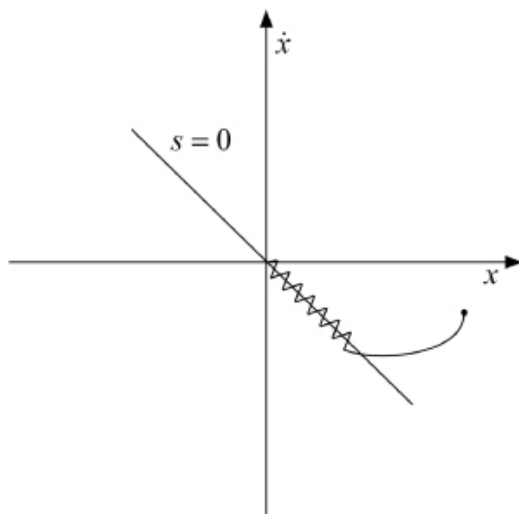


Figure 2.7: Representation of sliding mode control in state space. (Slotine et al. [1991])

First-order SMC is robust against bounded disturbances and is capable of achieving exponential convergence to a sliding mode within finite time. However, due to its discontinuous structure, the solution of the closed loop dynamics only exists in the Filippov sense. The discontinuity also has effects on SMC applications and performance. The SMC in theory requires infinite bandwidth and therefore is susceptible to a phenomenon called "chattering" in real world applications. The controller is expected to switch between input values instantaneously. This instantaneous switching about the sliding surface results in chattering. Chattering is undesirable and can cause damage to physical actuators and/or the system.

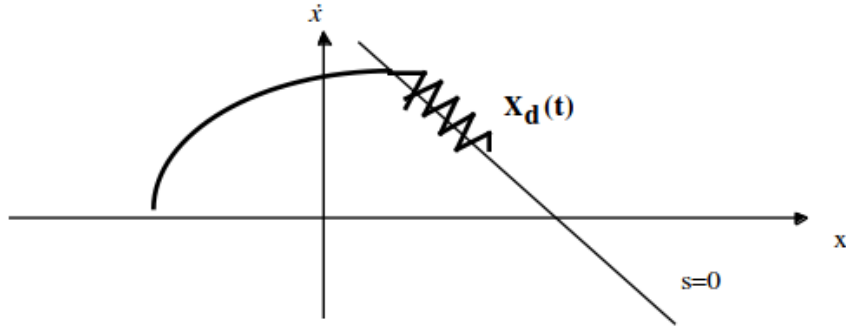


Figure 2.8: Chattering effect represented in state space. (Slotine et al. [1991])

In theory of sliding modes, the system stays on the sliding surface once it reaches it, and can be viewed as sliding only along the sliding surface. The real application of SMC approximates this theoretical behaviour with a high-frequency control signal that causes the system to chatter in a tight neighborhood of the sliding surface.

2.2.2.1 Existence of a Sliding Mode

For the given system, a sufficient condition of existence of a sliding mode is that

$$\dot{V} = \frac{\delta V}{\delta x} \frac{\delta x}{\delta t} = x^T \dot{x} < 0 \quad (2.23)$$

To achieve $x^T \dot{x} < 0$, the feedback control law $u(x)$ must be picked so that x and \dot{x} always have the opposite signs. A first-order SMC for the scalar nonlinear system given in (2.14) can be defined as

$$u(t) = -\beta \operatorname{sgn}(x) \quad (2.24)$$

where $\beta \in R^+$ is a positive constant control gain, and $\operatorname{sgn}()$ is the signum function. After substituting $u(t)$, into the dynamical system, the differential equation becomes

$$\dot{x} = f(x, t) - \beta \text{sgn}(x) \quad (2.25)$$

The time derivative of the Lyapunov function then becomes

$$\dot{V} = xf(x, t) - \beta|x| \quad \forall x \neq 0 \quad (2.26)$$

Based on (2.15) and (2.26), the control gain β is designed as:

$$\beta > \zeta \quad (2.27)$$

In order to ensure the sliding mode is reached in finite time, \dot{V} must be strongly bounded away from zero.

$$\dot{V} \leq -k(\sqrt{V})^\alpha \quad (2.28)$$

$$x\dot{x} \leq -k|x|^\alpha$$

Taking $\alpha = 1$ and rearranging terms,¹

$$x\dot{x} \leq -k|x| \quad (2.29)$$

$$\text{sgn}(x)\dot{x} \leq -k$$

This allows the control law to switch between positive and negative input depending on the sign of \dot{x} to ensure \dot{V} remains negative.

The Lyapunov derivative (2.26) is then upper bounded as:

¹Note: $\text{sgn}(x) = \frac{x}{|x|}$

$$\dot{V} \leq -k|x| \quad x \neq 0 \quad \text{or} \quad |x| > \epsilon \quad (2.30)$$

where $\epsilon \in R^+$ is an arbitrarily small constant and $k \in R^+$ is a constant satisfying the inequality $k \leq \beta - \zeta$ deduced from (2.15) and (2.26). Therefore, $W \triangleq 2\sqrt{V} = |x|$ satisfies the differential inequality

$$D^+W = \frac{1}{\sqrt{V}} \frac{dV}{dt} \leq -k \quad (2.31)$$

where D^+W is the upper right-hand derivative of W (i.e., Dini derivative).

Comparison lemma shows that

$$\frac{W(x) - W(x_0)}{t} \leq -k \quad (2.32)$$

$$W(x) \leq W(x_0) - kt$$

Thus, the trajectory reaches the sliding surface in finite time and once on the surface, it cannot leave.

2.3 Visual Servo Control

Visual Servo Control (VSC) can be defined as the use of computer vision data to control the motion of a mechanical system, e.g., a robot. VSC uses techniques from image processing, computer vision and control theory [Corke, 1996; Chaumette et al., 2007; Chaumette and Hutchinson, 2006]. Vision is a rich source of information and therefore is an attractive sensory option. However, the richness of information becomes

a disadvantage as well as it is an advantage. Visual data requires large amounts of memory for storage, and it is computationally costly. Fortunately, with the advancements in computational capabilities in the past decades, use of vision based systems has become a viable and attractive option for autonomous and tele-operated systems.

Visual systems acquire information using a camera. These systems are split into two categories based on the location of the camera with respect to the robot. The camera is either mounted directly on the robot, in which case the robot motion induces camera motion, or it is fixed somewhere in the workspace so that it can observe the robot from a stationary point of view. These configurations are known as *eye-in-hand* and *eye-to-hand* in the VSC community [Papanikolopoulos et al., 1991, 1993; Wijesoma et al., 1993; Hager et al., 1995; Chaumette and Hutchinson, 2006; Chaumette et al., 2007].

2.3.1 The Basics of Visual Servoing

Similar to common controllers, the aim of all vision-based control schemes is to minimize an error, $\mathbf{e}(t)$, which can be identified as:

$$\mathbf{e}(t) = \mathbf{s}(\mathbf{m}(t), \mathbf{a}) - \mathbf{s}^* \quad (2.33)$$

where $\mathbf{m}(t)$ represents a set of image measurements (i.e., image coordinates of interest points). These image measurements are used to compute a vector of visual features, $\mathbf{s} \in R^*$, in which \mathbf{a} is a set of parameters that contain additional knowledge about the system (i.e., camera intrinsic parameters, models of objects, etc.). The vector \mathbf{s}^*

represents the desired values of these features.

A simple velocity controller for a camera can be defined as

$$\dot{\mathbf{s}} = \mathbf{L}\nu_c \quad (2.34)$$

where $\nu_c = (v_c, \omega_c)$ is the velocity of the camera, $\mathbf{L} \in R^{k \times 6}$ is the interaction matrix (Jacobian, camera intrinsic parameters). Taking the time derivative of (2.33), the rate of error and $\dot{\mathbf{s}}$ can be related as

$$\dot{\mathbf{e}} = \mathbf{L}\nu_c \quad (2.35)$$

In this case, ν is considered to be the control input to the system. For an exponential decrease of the error, the error rate can be defined as:

$$\dot{\mathbf{e}} = -\lambda\mathbf{e} \quad (2.36)$$

Using (2.35) and (2.36), \mathbf{e} and ν_c are related as:

$$\nu_c = -\lambda\mathbf{L}^+\mathbf{e} \quad (2.37)$$

where $\mathbf{L}^+ \in R^{6 \times k}$ is the Moore-Penrose pseudo inverse of \mathbf{L} , ($\mathbf{L}^+ = (\mathbf{L}^T\mathbf{L})^{-1}$) when \mathbf{L} is of full rank 6. In real life situations it is impossible to exactly know \mathbf{L} , so an approximation or an estimate is used instead. The approximation of the pseudo-inverse of the interaction matrix is represented as $\widehat{\mathbf{L}}^+$. By this notation, the control law becomes

$$\nu_c = -\lambda\widehat{\mathbf{L}}^+\mathbf{e} \quad (2.38)$$

Based on how \mathbf{s} is chosen, VSC splits into two major schemes: Position-Based Visual Servoing (PBVS) and Image-Based Visual Servoing (IBVS).

2.3.2 Position-Based Visual Servo Control

Position-based control techniques use the pose of the camera with respect to a reference frame to define \mathbf{s} [Hutchinson et al., 1996; Malis et al., 1999; Corke and Hutchinson, 2001; Chaumette and Hutchinson, 2006; Chaumette et al., 2007]. In PBVS, features are extracted from the image to estimate/compute a partial 3D reconstruction of the target or motion of it in the environment. An error is calculated as the difference between the current pose and the desired pose in task space which is used by the control system (see Figure 2.9).

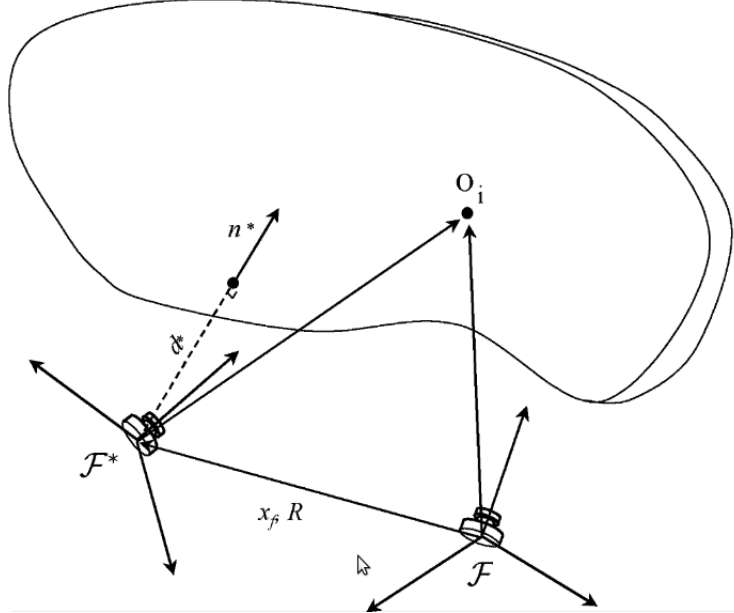


Figure 2.9: \mathcal{F} and \mathcal{F}^* represent current and desired camera frames. PBVS schemes use the difference between these frames to calculate an error to minimize. [Hu et al., 2009]

For some applications, the IBVS approach is more popular compared to PBVS schemes since position-based schemes rely on 3D reconstruction. Therefore any errors in the calibration of the vision system will subsequently lead to errors in task execution [Chaumette, 1998]. Position-based schemes also lack a mechanism by which the image is directly regulated. This can result in the feature points leaving the camera field of view. An IBVS control law directly links image space velocities to velocities in the robot work space. This means the robot is directly actuated using the measurements from the image. In return, computational delay is reduced and the necessity for image interpretation is eliminated. Furthermore, image-based schemes are robust to camera calibration and sensor modelling error.

2.3.3 Image-Based Visual Servo Control

Classically, coordinates of feature points projected onto the image plane are used to define the set \mathbf{s} in image-based control schemes. The image measurement set \mathbf{m} is not necessarily limited to image points (i.e., image moments [Mebarki et al., 2010; Copot et al., 2012]). The parameter set \mathbf{a} is the *camera intrinsic parameters* which relate the feature points to the image plane (i.e., projection model). The properties of the projection model are translated through the interaction matrix.

2.3.3.1 The Interaction Matrix

A point in a 3D Euclidean space with coordinates $\mathbf{X} = (X, Y, Z)$, is projected to the image plane as a 2D point with coordinates $\mathbf{x} = (x, y)$ through the pinhole lens model.

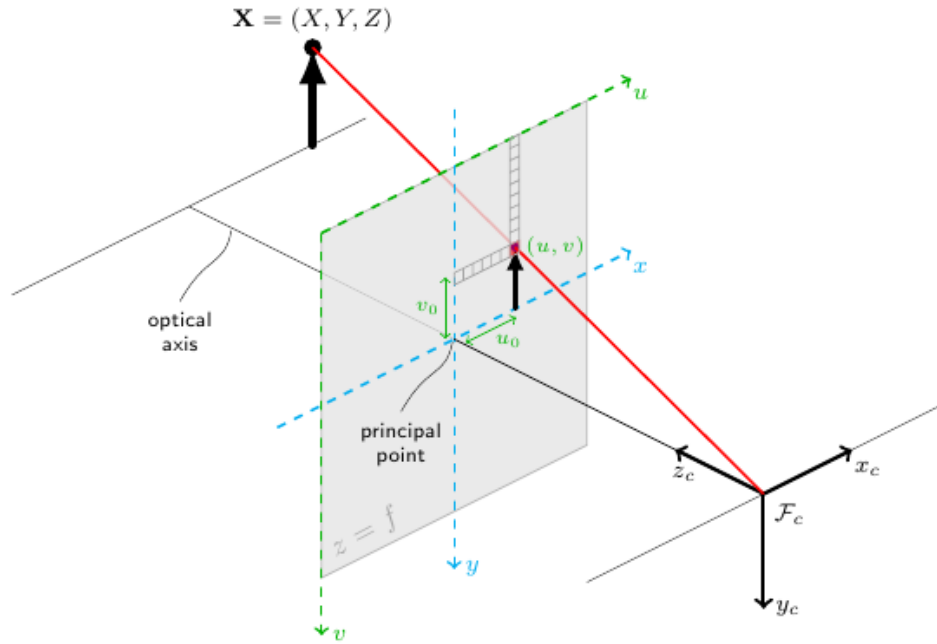


Figure 2.10: Camera projection model displaying the Euclidean space and image space relation.

Considering the scenario depicted in Figure 2.10, simple geometry can be used to obtain

$$x = \frac{X}{Z} = (u - u_0)/f \tag{2.39}$$

$$y = \frac{Y}{Z} = (v - v_0)/f$$

where $\mathbf{m} = (u, v)$ are the coordinates of the point expressed in pixel units, u_0 and v_0 are the coordinates of the principal point, a and b are camera scaling factors along x, y -axes and f is the focal length of camera. In this case, the visual feature set is selected as the coordinates of the image point (i.e., $\mathbf{s} = \mathbf{x} = (x, y)$).

Taking the time derivative of (2.39) provides:

$$\dot{x} = \frac{\dot{X}Z - X\dot{Z}}{Z^2} = (u - u_0)/f \quad (2.40)$$

$$\dot{y} = \frac{\dot{Y}Z - Y\dot{Z}}{Z^2} = (v - v_0)/f$$

Then the velocity of the 3D point can be related to the camera spatial velocity by:

$$\dot{\mathbf{X}} = -v_c - \omega_c \times \mathbf{X} \quad (2.41)$$

where

$$\begin{aligned} \dot{X} &= -v_x - \omega_y Z + \omega_z Y \\ \dot{Y} &= -v_y - \omega_z X + \omega_x Z \\ \dot{Z} &= -v_z - \omega_x Y + \omega_y X \end{aligned} \quad (2.42)$$

After using (2.42) in (2.40), with some factoring and simplification, $\dot{\mathbf{x}}$ can be represented in the following form,

$$\dot{\mathbf{x}} = \mathbf{L}v_c \quad (2.43)$$

where \mathbf{L} is the interaction matrix defined as

$$\mathbf{L} = \begin{bmatrix} -\frac{1}{Z} & 0 & \frac{x}{Z} & xy & -(1+x^2) & y \\ 0 & -\frac{1}{Z} & \frac{y}{Z} & (1+y^2) & -xy & -x \end{bmatrix} \quad (2.44)$$

Chapter 3

Dynamic and Kinematic Models

3.1 Coordinate Frames

The dynamic system being modeled consists of multiple components: the 3D space where the motion takes place, the missile and target, and the camera used for tracking the target. In order to relate subcomponents of the system, the following coordinate frames are defined.

3.1.1 Missile Frame

An orthogonal frame $\mathcal{F}_m(t)$ is defined at the center of gravity (CoG) of the missile.

3.1.2 Earth-Fixed Frame

An Earth-fixed reference frame \mathcal{F}_e is defined on the surface of the Earth which is used to track the motion of the missile and target in 3D space.

3.1.3 Reference Frame

A body carried reference frame \mathcal{F}_r is defined, located at the CoG of the missile. Frame \mathcal{F}_r is fixed to a North-East-Down (NED) navigation frame, and is assumed to coincide with frame \mathcal{F}_e (assuming the Earth's curvature is negligible). The body-carried reference frame \mathcal{F}_r is used to define the angular orientation of the aircraft while the Earth-fixed reference frame \mathcal{F}_e is used to define its translation.

3.1.4 Camera Frame

A monocular camera would most likely be located at the nose of the missile. However for model simplification, the camera frame $\mathcal{F}_c(t)$ is defined at the center of gravity of the missile, coinciding with the frames $\mathcal{F}_m(t)$ and \mathcal{F}_r . If necessary, this can easily be changed by adding the translation between the nose and the CoG to \mathcal{F}_c

3.2 Missile Dynamics

The dynamic model for a bank-to-turn missile (BTT) is used in the subsequent control development. The orientation of frame \mathcal{F}_m with respect to frame \mathcal{F}_r is defined by the angles of rotation $\phi(t)$, $\sigma(t)$, and $\psi(t)$ about the x , y , and z axes, respectively.

The linear and angular velocities of the missile measured in \mathcal{F}_m with respect to \mathcal{F}_e are denoted by

$$v_m = [v_x \quad v_y \quad v_z]^T \in \mathbb{R}^3 \quad (3.1)$$

$$\omega_m = [\omega_x \quad \omega_y \quad \omega_z]^T \in \mathbb{R}^3 \quad (3.2)$$

3.2.1 Linear Acceleration

The linear acceleration of the missile measure in the body frame $\mathcal{F}_m(t)$ is expressed as

$$\dot{v}_x = \omega_z v_y - \omega_y v_z + \frac{F_x}{m} \quad (3.3)$$

$$\dot{v}_y = \omega_x v_z - \omega_z v_x + \frac{F_y}{m} \quad (3.4)$$

$$\dot{v}_z = \omega_y v_x - \omega_x v_y + \frac{F_z}{m}. \quad (3.5)$$

In the equations above, $m \in \mathbb{R}$ represents the constant mass of the missile, and $F_x(t), F_y(t), F_z(t) \in \mathbb{R}$ are the forces acting along the body axes defined as

$$F_x = G_x(q) + k_F \rho_{air} V_M^2 C_x(\alpha, \beta, M_m) + \tau_x \quad (3.6)$$

$$F_y = G_y(q) + k_F \rho_{air} V_M^2 C_y(\alpha, \beta, M_m) + \tau_y \quad (3.7)$$

$$F_z = G_z(q) + k_F \rho_{air} V_M^2 C_z(\alpha, \beta, M_m) + \tau_z \quad (3.8)$$

where $k_F \in \mathbb{R}$ is a constant parameter determined by the missile geometry, $\rho_{air} \in \mathbb{R}$ is the air density, and $V_M(t) \in \mathbb{R}$ is the magnitude of the missile velocity measured with respect to \mathcal{F}_e . $C_x(\alpha, \beta, M_m)$, $C_y(\alpha, \beta, M_m)$, $C_z(\alpha, \beta, M_m) \in \mathbb{R}$ are the unknown friction coefficients corresponding to the aerodynamic forces, where $\alpha(t)$, $\beta(t)$, $M_m(t)$ represent the angle of attack, sideslip angle, and Mach number, respectively. $\tau_x, \tau_y, \tau_z \in \mathbb{R}$ are the control force inputs ¹. The x, y , and z components of the gravitational force acting on the missile, $G_x(t)$, $G_y(t)$, $G_z(t) \in \mathbb{R}$ are expressed as

$$G_x(t) = -mg \sin(\sigma) \tag{3.9}$$

$$G_y(t) = -mg \cos(\sigma) \sin(\phi) \tag{3.10}$$

$$G_z(t) = -mg \cos(\sigma) \cos(\phi) \tag{3.11}$$

where $g \in \mathbb{R}$ is the gravitational acceleration constant.

¹It should be noted that the control force input, $\tau = [\tau_x \ \tau_y \ \tau_z \ \tau_l \ \tau_m \ \tau_n]^T$, is assumed to be decoupled in this preliminary study (i.e., the control input can be applied in 6-DoF independently). The 6-DoF independent control is commonly used in order to simplify the dynamic model (Mehta et al. [2011], Mehta et al. [2012b], Mehta et al. [2012a]). However, use of a realistic dynamic model is intended for future studies in which deflection surface angles are used to steer the missile (Yanushevsky [2007]).

3.2.2 Angular Acceleration

The angular acceleration of the missile measured in \mathcal{F}_m with respect to \mathcal{F}_e is denoted by

$$\dot{\omega}_x = \frac{I_y - I_z}{I_x} \omega_y \omega_z + \frac{L}{I_x} \quad (3.12)$$

$$\dot{\omega}_y = \frac{I_z - I_x}{I_y} \omega_x \omega_z + \frac{M}{I_y} \quad (3.13)$$

$$\dot{\omega}_z = \frac{I_x - I_y}{I_z} \omega_x \omega_y + \frac{N}{I_z} \quad (3.14)$$

where $I_x, I_y, I_z \in \mathbb{R}$ denote the constant unknown moments of inertia about x, y , and z -axes. $L(t), M(t), N(t) \in \mathbb{R}$ are the rolling, pitching and yawing moments, respectively, given by

$$L = k_M \rho_{air} V_M^2 C_l(\alpha, \beta, M_m) + \tau_l \quad (3.15)$$

$$M = k_M \rho_{air} V_M^2 C_m(\alpha, \beta, M_m) + \tau_m \quad (3.16)$$

$$N = k_M \rho_{air} V_M^2 C_n(\alpha, \beta, M_m) + \tau_n. \quad (3.17)$$

$C_l(\alpha, \beta, M_m), C_m(\alpha, \beta, M_m), C_n(\alpha, \beta, M_m) \in \mathbb{R}$ are the unknown coefficients of friction corresponding to the aerodynamic moments, and $\tau_l, \tau_m, \tau_n \in \mathbb{R}$ are control moment inputs. The friction coefficients in (3.6,3.15) can be linearly parametrized in terms of linear velocities $v_x(t), v_y(t)$, and $v_z(t)$ for small angles of $\alpha(t)$ and $\beta(t)$ as

$$C_i = C_{i0} + C_{i\beta} \frac{v_y}{v_x} + C_{i\alpha 1} \frac{v_z}{v_x} + C_{i\alpha 2} \left(\frac{v_z}{v_x} \right)^2 \quad (3.18)$$

$$+ C_{i\alpha 3} \left(\frac{v_z}{v_x} \right)^3 + C_{iM_1} \left(\frac{v_x}{v_s} \right) + C_{iM_2} \left(\frac{v_z}{v_s} \right) \quad (3.19)$$

$$+ C_{iM_3} \left(\frac{v_z^2}{v_x v_s} \right) + C_{iM_4} \left(\frac{v_z^3}{v_x^2 v_s} \right) \quad (3.20)$$

where $v_s(t) \in \mathbb{R}$ denotes the local speed of sound, and $C_{i0}, C_{i\beta}, C_{i\alpha1}, C_{i\alpha2}, C_{i\alpha3}, C_{iM1}, C_{iM2}, C_{iM3}, C_{iM4} \in \mathbb{R}$ are unknown constant friction parameters, for $i = x, y, z, l, m$, or n .

3.2.3 Equation of Motion

The equation of motion for the missile can now be expressed in Euler-Lagrange form, considering the coordinate frames and dynamical equations defined above, as

$$M\ddot{q} = C(\dot{q})\dot{q} + G(q) + f(\dot{q}) + \tau + \tau_d \quad (3.21)$$

where $q(t), \dot{q}(t) \in \mathbb{R}^6$ denote the 6-DOF position and velocity, respectively, of frame $\mathcal{F}_m(t)$ with respect to frame \mathcal{F}_e where

$$q(t) = [x \ y \ z \ \phi \ \sigma \ \psi]^T \quad (3.22)$$

$$\dot{q}(t) = [v_m^T \ \omega_m^T]. \quad (3.23)$$

In equation (3.21), $\tau_d(t) \in \mathcal{R}^6$ denotes an unknown, nonlinear, nonvanishing bounded disturbance, while $M \in \mathbb{R}^{6 \times 6}$ represents the unknown constant inertia matrix, $C(\dot{q}) \in \mathbb{R}^{6 \times 6}$ is the Coriolis matrix, $G(q) \in \mathbb{R}^6$ is the unknown gravity vector, and $f(\dot{q}) \in \mathbb{R}^6$ denotes the unknown friction vector, which are defined as

$$M = \text{diag}(m, m, m, I_x, I_y, I_z), \quad C(\dot{q}) = \text{diag}(-[m\omega_m]_{\times}, [mv_m]_{\times}) \quad (3.24)$$

$$G(q) = \begin{bmatrix} -mg \sin(\sigma) \\ mg \cos(\sigma) \sin(\phi) \\ mg \cos(\sigma) \cos(\phi) \\ 0 \\ 0 \\ 0 \end{bmatrix}, \quad f(\dot{q}) = \begin{bmatrix} k_F \rho_{air} v_x^2 C_x \\ k_F \rho_{air} v_x^2 C_y \\ k_F \rho_{air} v_x^2 C_z \\ k_F \rho_{air} v_x^2 C_l \\ k_F \rho_{air} v_x^2 C_m \\ k_F \rho_{air} v_x^2 C_n \end{bmatrix} \quad (3.25)$$

In equation (1.27), $diag(\cdot)$ represents a diagonal matrix, and $[\cdot]_{\times}$ represents the skew-symmetric cross-product matrix.

3.3 Image Kinematics

This section formulates the relationships between the missile velocity $\dot{q}(t) \in \mathbb{R}^6$ and the velocity of the target \mathcal{T} in the camera image plane. A monocular camera is attached to the center of gravity of the missile airframe.

Note 2 *Although the camera is placed at the nose of the missile in real life, this assumption can be made without the loss of generality, since any deviation can be accounted for by a simple coordinate transformation.*

A time-varying orthogonal frame $\mathcal{F}_c(t)$ is attached to the camera such that the origins of $\mathcal{F}_c(t)$ and missile body frame \mathcal{F}_m coincide with the missile center of gravity. A target \mathcal{T} is represented as a point in the Euclidean space and it is assumed to remain in the camera field of view.²

²This is to ensure the closed-loop behavior of the system. Some existing vision-based controllers have a potential field implemented around the FOV within the control law to ensure feature points stay on the image plane. (Corke and Hutchinson [2001])

Euclidean coordinates of the target \mathcal{T} expressed in the camera coordinate frame $\mathcal{F}_c(t)$ can be represented as

$$\bar{m}(t) \triangleq [x_t(t) \quad y_t(t) \quad z_t(t)]^T \quad (3.26)$$

where it is assumed that the target is always in front of the camera (i.e., $z_t(t) > \epsilon, \epsilon \in \mathbb{R}^+$). The rate of change of the Euclidean coordinates $\bar{m}(t)$ due to the camera motion is related to the camera velocity as [Mehta et al., 2012a]

$$\dot{\bar{m}}(t) = -v_c(t) - \omega_c(t) \times \bar{m}(t) \quad (3.27)$$

where $v_c(t), \omega_c(t) \in \mathbb{R}^3$ are linear and angular velocities of the camera as measured in \mathcal{F}_c respectively. Using transformation of left-hand coordinate frame to right-hand coordinate frame, left-handed camera coordinate frame can be related to the 6-DOF missile velocity as measured in \mathcal{F}_m as

$$v_c = [v_y \quad -v_z \quad v_x]^T \quad \text{and} \quad \omega = [\omega_y \quad -\omega_z \quad \omega_x]^T \quad (3.28)$$

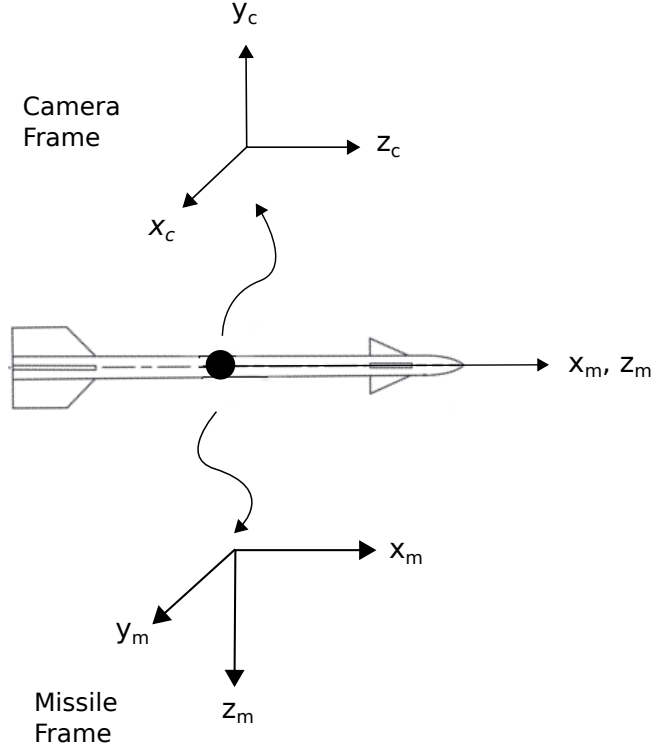


Figure 3.2: Left-handed camera and right-handed missile frames located at the CoG.

The target \mathcal{T} is projected onto an image plane π as the point

$$p(t) \triangleq [u(t) \quad v(t)]^T \quad (3.29)$$

where pixel coordinates $p(t)$ are related to the Euclidean coordinates $\bar{m}(t)$ via projection geometry as

$$u(t) = \frac{f a x_t(t)}{z_t(t)} + u_0 \quad v(t) = \frac{f b y_t(t)}{z_t(t)} + v_0 \quad (3.30)$$

where $f \in \mathbb{R}$ is the focal length, a and $b \in \mathbb{R}$ are scaling factors along x and y-axes; $[u_0 v_0]^T \in \mathbb{R}^2$ are the principal point coordinates (i.e., the intersection of an optical axis with the image plane) of the camera. Taking the time derivative of $p(t)$, the

following expression for the rate of change of the pixel coordinates is obtained:

$$\dot{p}(t) = \begin{bmatrix} \dot{u} \\ \dot{v} \end{bmatrix} = f \begin{bmatrix} a \\ b \end{bmatrix} \begin{bmatrix} \frac{\dot{x}z - x\dot{z}}{z^2} \\ \frac{\dot{y}z - y\dot{z}}{z^2} \end{bmatrix} \quad (3.31)$$

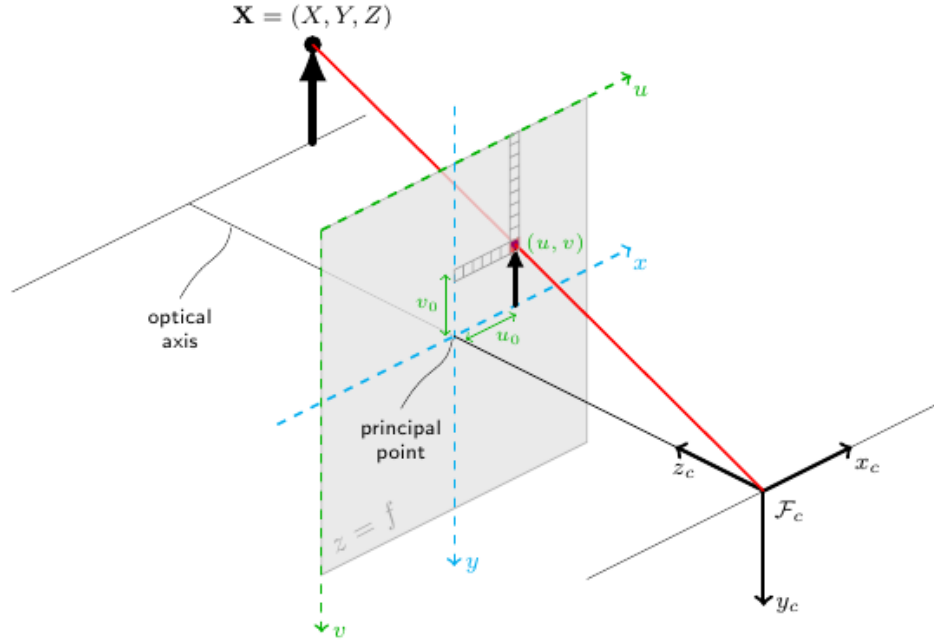


Figure 3.3: Camera projection model displaying the Euclidean space and image space relation.

Substituting $\dot{x}, \dot{y}, \dot{z}$ from \dot{m} into the equation above and factoring out $\frac{1}{z^2}$, the equation becomes

$$\dot{p}(t) = f \begin{bmatrix} a \\ b \end{bmatrix} \frac{1}{z^2} \begin{bmatrix} -v_y z_t + \omega_z z_t^2 + \omega_x y_t z_t + x_t v_x + x_t \omega_y y_t + x_t^2 \omega_z \\ v_z z_t + \omega_y z_t^2 - \omega_x x_t z_t + y_t v_x + y_t^2 \omega_y + y_t \omega_z x_t \end{bmatrix} \quad (3.32)$$

Then linear and angular acceleration terms can be factored out to give

$$\dot{p}(t) = \begin{bmatrix} \frac{f a x_t}{z_t^2} & -\frac{f a}{z_t} & 0 & \frac{f a y_t}{z_t} & \frac{f a x_t y_t}{z_t^2} & a(f + \frac{f x_t^2}{z_t^2}) \\ \frac{f b y_t}{z_t^2} & 0 & \frac{f b}{z_t} & -\frac{f b x_t}{z_t} & b(f + \frac{f y_t^2}{z_t^2}) & \frac{f b x_t y_t}{z_t^2} \end{bmatrix} \begin{bmatrix} v_x \\ v_y \\ v_z \\ \omega_x \\ \omega_y \\ \omega_z \end{bmatrix} \quad (3.33)$$

This relation can be simplified to the following form which relates velocities in Euclidean space to the feature point velocities in the image

$$\dot{p}(t) = \begin{bmatrix} \dot{u}(t) \\ \dot{v}(t) \end{bmatrix} = J \dot{q}(t) \quad (3.34)$$

where $J \in \mathbb{R}^{2 \times 6}$ denotes the Jacobian matrix which contains the projection geometry as explained earlier in the Visual Servo Control section.

$$J = \begin{bmatrix} \frac{f a x_t}{z_t^2} & -\frac{f a}{z_t} & 0 & \frac{f a y_t}{z_t} & \frac{f a x_t y_t}{z_t^2} & a(f + \frac{f x_t^2}{z_t^2}) \\ \frac{f b y_t}{z_t^2} & 0 & \frac{f b}{z_t} & -\frac{f b x_t}{z_t} & b(f + \frac{f y_t^2}{z_t^2}) & \frac{f b x_t y_t}{z_t^2} \end{bmatrix} \quad (3.35)$$

The estimation of depth is a challenge using a monocular camera. In this dissertation, any uncertainties due to inaccurate depth information are assumed to be absorbed into the unknown auxiliary terms \tilde{N} and N_d , which are introduced in the Control Development section. These terms are compensated by the robust control law design. Future work might consider using a homography-based approach, which utilizes minimal information about the target in order to calculate the depth information (Hu et al. [2009], Mackunis et al. [2007]).

Remark 1 *The image Jacobian J given above remains bounded everywhere except at $z_t = 0$. This occurs when the camera frame \mathcal{F}_c intercepts the target \mathcal{T} . However, the impact actually happens before \mathcal{F}_c intercepts the target which is attached to the missile CoG for practical purposes. Therefore the missile is considered to have intercepted the target when $0 < z_t \leq z_{min}, z_{min} \in \mathbb{R}^+$.*

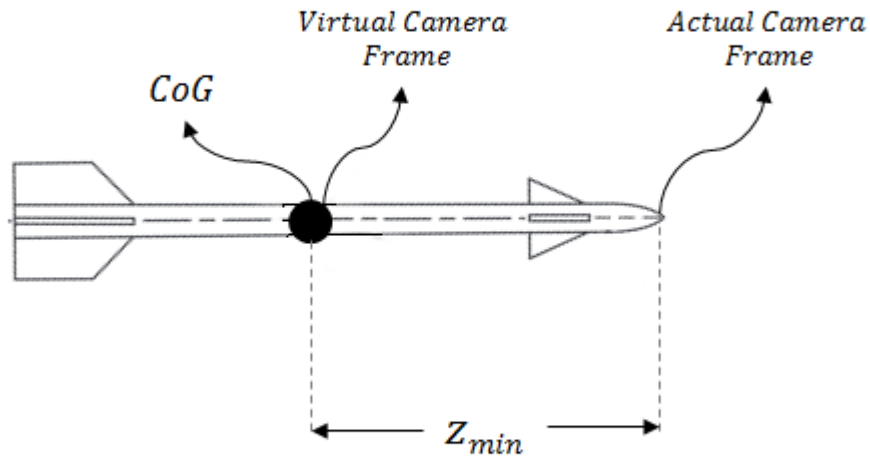


Figure 3.4: Actual camera position vs. virtual camera position. The missile is assumed to have intercepted the target if the relative distance z_t is equal to or less than z_{min} .

Chapter 4

Control System

4.1 Control Objective

The control objective of this system is to drive the relative distance between the missile frame \mathcal{F}_m and the target \mathcal{T} to zero, or to intercept the target in other words. This can be achieved by driving the time-varying target pixel coordinates $p(t)$ to the desired image coordinates p_d . Therefore, the control objective can be mathematically stated as:

$$p(t) \longrightarrow p_d \quad \text{where,} \quad p_d = [u_0 \quad v_0]^T \quad (4.1)$$

4.2 Control Development

Property 1: The inertia matrix M is symmetric, positive definite, such that for known positive constants $m_1, m_2 \in \mathbb{R}$, the following inequality is satisfied:

$$m_1 \|\xi^2\| \leq \xi^T M \xi \leq m_2 \|\xi^2\| \quad \forall \xi \in \mathbb{R}^n \quad (4.2)$$

A tracking error term $e(t) \triangleq [e_1 \ e_2]^T \in \mathbb{R}^2$ is defined based on the control objective as the difference between the image coordinates of target and the principal point.

$$e(t) \triangleq p_d - p(t) \quad (4.3)$$

Taking the time derivative of the error term and using the image kinematic equation from (3.34), we obtain

$$\dot{e}(t) = -\dot{p}(t) = -J\dot{q} \quad (4.4)$$

For the subsequent control development and stability analysis, we add and subtract λe to the equation above

$$\dot{e}(t) = -J\dot{q} + \lambda e - \lambda e \quad (4.5)$$

where $\lambda \in \mathbb{R}$ is a positive constant. An auxiliary error term $r(t) \in \mathbb{R}^6$ is introduced to facilitate the following controller development and stability analysis

$$r(t) = -\dot{q} + J^+ \lambda e \quad (4.6)$$

where $J^+(t) \in \mathbb{R}^{6 \times 2}$ denotes the pseudo-inverse of the Jacobian matrix $J(t)$. By using (4.5) and (4.6), the rate of change of the error term $e(t)$ then can be expressed as

$$\dot{e}(t) = -\lambda e + Jr \quad (4.7)$$

First by pre-multiplying the auxiliary error signal $r(t)$ and then taking the time derivative of this term results in the following expression for open-loop dynamics:

$$M\dot{r} = -M\ddot{q} + MJ^+\lambda e + MJ^+\lambda \dot{e} \quad (4.8)$$

By substituting the dynamics equation in (3.21), the open-loop error dynamics can be expressed as

$$M\dot{r} = -J^T e - \tau + \tilde{N} + N_d \quad (4.9)$$

where

$$\begin{aligned} \tilde{N} = & -C\dot{q} + C\dot{q}_d - G(q) + G(q_d) \\ & -f(\dot{q}) + f(\dot{q}_d) + MJ^+\lambda e - MJ^+(q_d)\lambda e \\ & + MJ^+\lambda \dot{e} - MJ^+\lambda \dot{e}(q_d) + J^T e - J^T(q_d)e \end{aligned} \quad (4.10)$$

and

$$\begin{aligned} N_d = & -C\dot{q}_d - G(q_d) - f(\dot{q}_d) + MJ^+(q_d)\lambda e \\ & + MJ^+\lambda \dot{e}(q_d) + J^T(q_d)e + \tau_d \end{aligned} \quad (4.11)$$

The selective grouping of the terms in (4.10) and (4.11) is motivated by the fact that the following bounding inequalities can be developed [MacKunis et al., 2010a, b]:

$$\|\tilde{N}\| \leq \rho(\|z\|)\|z\| \quad , \quad \|N_d\| \leq \zeta_d \quad (4.12)$$

where $\rho, \zeta_d \in \mathbb{R}$ are known positive bounding constants, and z is an error vector defined as

$$z(t) \triangleq [e^T \quad r^T]^T \quad (4.13)$$

Based on the open-loop error system and the subsequent stability analysis, the control input τ is designed as

$$\tau = (k_s + 1)r + \beta \text{sgn}(r) \quad (4.14)$$

where $k_s \in \mathbb{R}$ and $\beta \in \mathbb{R}$ are positive constants and $\text{sgn}(\cdot)$ is the signum function.

The closed-loop error system can then be obtained by substituting the control input expression into the open-loop error system in (4.9) as

$$M\dot{r} = \tilde{N} + N_d - J^T e - (k_s + 1)r - \beta \text{sgn}(r) \quad (4.15)$$

Chapter 5

Stability Analysis

Theorem 4 *The controller presented in (4.14) ensures that the missile airframe F_m intercepts the target in the following mathematical sense.*

$$\lim_{t \rightarrow \infty} r(t), e(t) = 0 \quad (5.1)$$

Proof 1 *Consider a non-negative Lyapunov function, $V(t)$, defined as:*

$$V(t) = \frac{1}{2}r^T M r + \frac{1}{2}e^T e \quad (5.2)$$

Taking the time derivative of $V(t)$ yields

$$\dot{V} = r^T M \dot{r} + e^T \dot{e} \quad (5.3)$$

Substituting (4.5) and (4.15) into the equation above, \dot{V} can be expressed as

$$\dot{V} = r^T (\tilde{N} + N_d - \tau - \frac{1}{2}M\dot{r} - J^T e) + e^T (Jr - \lambda e) \quad (5.4)$$

After cancelling common terms and substituting the control input τ , the following equation is obtained.

$$\dot{V} = r^T \tilde{N} + r^T N_d - r^T (k_s + 1)r - r^T \beta \text{sgn}(r) - e^T \lambda e \quad (5.5)$$

Based on the bounding inequalities defined in (4.12), $\dot{V}(e, r)$ can be upper bounded as:

$$\dot{V} \leq [\|r\| \rho(\|z\|) \|z\| - \|r\|^2 k_s] + \|r\| \zeta_d - \|r\|^2 - \beta \|r\| - \lambda \|e\|^2 \quad (5.6)$$

After completing the square for the terms in brackets and then reorganizing, the Lyapunov derivative can be expressed as

$$\begin{aligned} \dot{V} \leq & -k_s \left(\|r\|^2 - \frac{\rho(\|z\|) \|r\| \|z\|}{k_s} + \frac{\rho^2(\|z\|) \|z\|^2}{4k_s^2} \right) \\ & + \frac{\rho^2(\|z\|) \|z\|^2}{4k_s} + (\zeta_d - \beta) \|r\| - \|r\|^2 - \lambda \|e\|^2 \end{aligned} \quad (5.7)$$

where the control gain β is designed as $\beta > \zeta_d$.

Thus, the Lyapunov derivative can be upper bounded as

$$\dot{V} \leq \frac{\rho^2(\|z\|) \|z\|^2}{4k_s} - \|r\|^2 - \lambda \|e\|^2 \quad (5.8)$$

Using equation (4.13), the upper bound on \dot{V} can be expressed as

$$\dot{V} \leq -\lambda_0 \|z\|^2 + \frac{\rho^2(\|z\|) \|z\|^2}{4k_s} \quad (5.9)$$

where $\lambda_0 \triangleq \min\{1, \lambda\}$. Thus, based on (5.9), $\dot{V}_L \leq 0$ for $\|z\| \in \mathcal{D}$, where \mathcal{D} is defined as

$$\mathcal{D} \triangleq \{z(t) \in \mathcal{D} \mid \|z\| \leq \rho^{-1}(2\sqrt{\lambda_0 k_s})\}$$

Thus, asymptotic stability is achieved provided $z(t)$ remains in the set \mathcal{D} , where \mathcal{D} can be made arbitrarily large by increasing the control gain k_s ; i.e., a semi-global asymptotically stable (SGAS) result. Hence, for $\|z\| \in \mathcal{D}$, the upper bound on the Lyapunov derivative can be expressed as

$$\dot{V} \leq -c\|z\|^2 \tag{5.10}$$

where $c \in \mathbb{R}$ is a positive bounding constant.

The inequality (5.9) can be used to show that $V(e, r) \in \mathcal{L}_\infty$ in \mathcal{D} . Likewise, using (5.2), it can be concluded that $e(t), r(t) \in \mathcal{L}_\infty$ in \mathcal{D} . By using this conclusion and equation (4.5), it must be that $\dot{e}(t) \in \mathcal{L}_\infty$ in \mathcal{D} . Since $\dot{e}(t) = -\dot{p}(t)$, $\dot{p}(t) \in \mathcal{L}_\infty$ in \mathcal{D} . From standard linear analysis, it can then be proven that $\dot{q}(t) \in \mathcal{L}_\infty$ in \mathcal{D} . Given that $r(t) \in \mathcal{L}_\infty$, the control input $\tau(t) \in \mathcal{L}_\infty$ in \mathcal{D} . These can be used along with the closed-loop dynamic equation (4.15) to conclude that $q(t) \in \mathcal{L}_\infty$ in \mathcal{D} .

Chapter 6

Simulation - Stationary Target

The performance of the proposed robust control law was tested via numerical computer simulation using Matlab. The first simulation involved a stationary target located at a Euclidean point, $t_t \in \mathcal{R}^3$, with respect to the NED earth frame given by

$$t_t = [1200 \quad 2400 \quad -5000]^T(m) \quad (6.1)$$

A missile body frame, \mathcal{F}_m , is defined at initial position

$$t_m = [0 \quad 0 \quad -3500]^T \quad (6.2)$$

and initial orientation,

$$R_m = \begin{bmatrix} 0.5000 & -0.8138 & 0.2942 \\ 0.8660 & 0.4698 & -0.1710 \\ 0 & 0.3420 & 0.9397 \end{bmatrix} \quad (6.3)$$

The constant modeling parameters are defined below [Mehta et al. [2012a]].

$$\begin{aligned}
m &= 144.0 \quad [kg] & g &= 9.81 & [m/s^2] \\
I_x &= 1.615 \quad [kg - m^2] & \rho_{air} &= 0.26 & [kg/m^3] \\
I_y &= 136.0 \quad [kg - m^2] & k_F &= 0.01425 & [m^2] \\
I_z &= 136.0 \quad [kg - m^2] & k_M &= 2.716 \times 10^{-3} & [m^3] \\
k_s &= 500 \quad [\cdot] & \beta_s &= 500 & [\cdot]
\end{aligned} \tag{6.4}$$

where m is mass of the missile, g is the gravitational acceleration, I_x, I_y, I_z are missile moment of inertia around x, y, z -axis respectively. Density of air is represented by ρ_{air} , while k_F and k_M are constant missile parameters. The missile and target velocities are initialized as

$$\dot{q} = [120 \quad 0 \quad 0 \quad 0 \quad 0 \quad 0]^T [m/s], \quad \dot{q}_t = [0 \quad 0 \quad 0 \quad 0 \quad 0 \quad 0]^T [m/s] \tag{6.5}$$

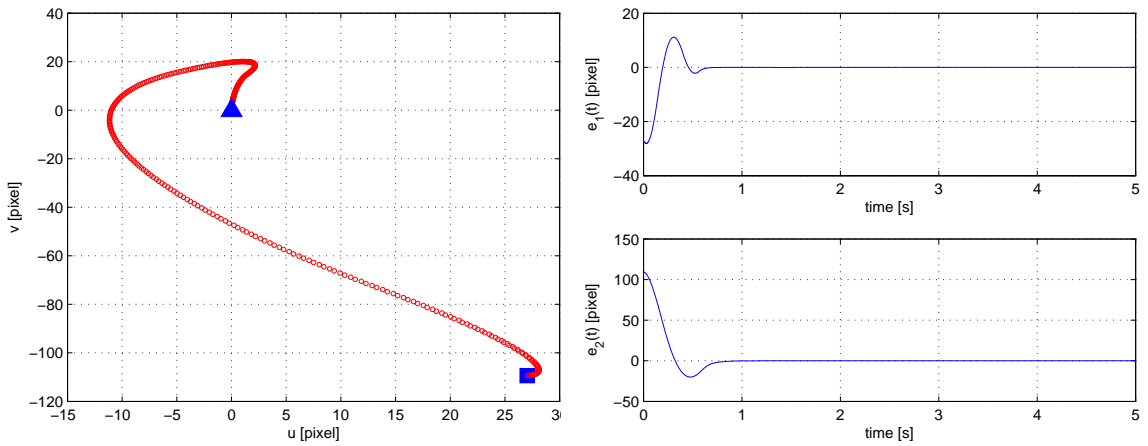
Friction coefficients are obtained by using,

$$\begin{aligned}
C_x &= -0.57 + 0.0083\alpha \\
C_y &= -0.21\beta \\
C_z &= (0.0429 - 0.5052\alpha + 0.0125\alpha^2 - 0.0015\alpha^3) \\
&\quad + (-0.0191 - 0.1230\alpha - 0.0138\alpha^2 + 0.0006\alpha^3)M_m \\
C_l &= 0.116\beta \\
C_m &= (-0.0381 - 2.7419\alpha + 0.2131\alpha^2 - 0.0055\alpha^3) \\
&\quad + (-0.4041 + 0.8715\alpha - 0.0623\alpha^2 + 0.0014\alpha^3)M_m \\
C_n &= 0.08\beta
\end{aligned} \tag{6.6}$$

The coefficients of friction (6.6) and the missile dynamic parameters are used only to generate the plant model and are not used in the guidance law. The simulation has additive white Gaussian noise (AWGN) in the target pixel coordinate $p(u, v)$ with

standard deviation of 0.1 pixel and the depth measurement $z(t)$ by 10m. The robust control law compensates for the unmodeled effects and AWGN added into the system.

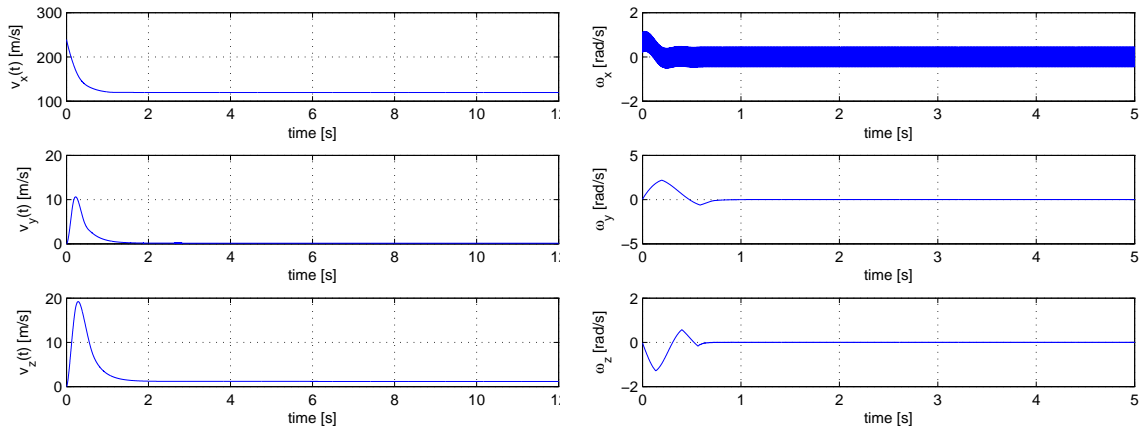
The figure below displays the tracking and error minimization performance of the proposed controller. Figure 6.1a shows the initial target position (\square) and the final position of the target (\triangle) in the image plane. Figure 6.1b displays the difference values between current and desired values of u and v , which were defined as the tracking error $e(t)$.



(a) Tracking

(b) Error in u and v

Figure 6.1: Tracking and error minimization performance is displayed for a stationary target.



(a) Linear velocities of the missile

(b) Angular velocities of the missile

Figure 6.2: Linear and angular velocities of the missile along x, y , and z – axis measured with respect to the earth frame.

Figure 6.2 shows the linear and angular velocities of the missile airframe during the tracking process measured with respect to NED earth frame. The force and moment inputs to the system during target tracking are plotted in Figure 6.3.

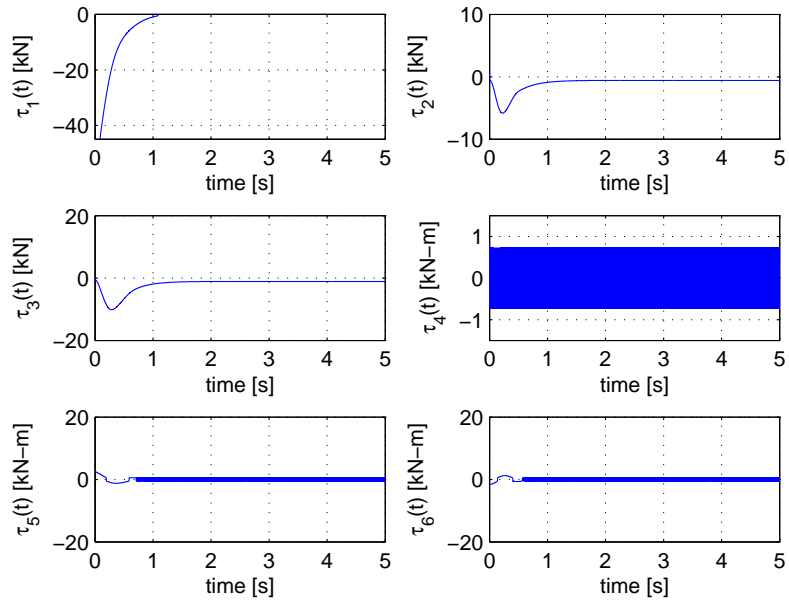


Figure 6.3: This plot shows the control input ($\tau(t)$) applied to the missile airframe during the simulation.

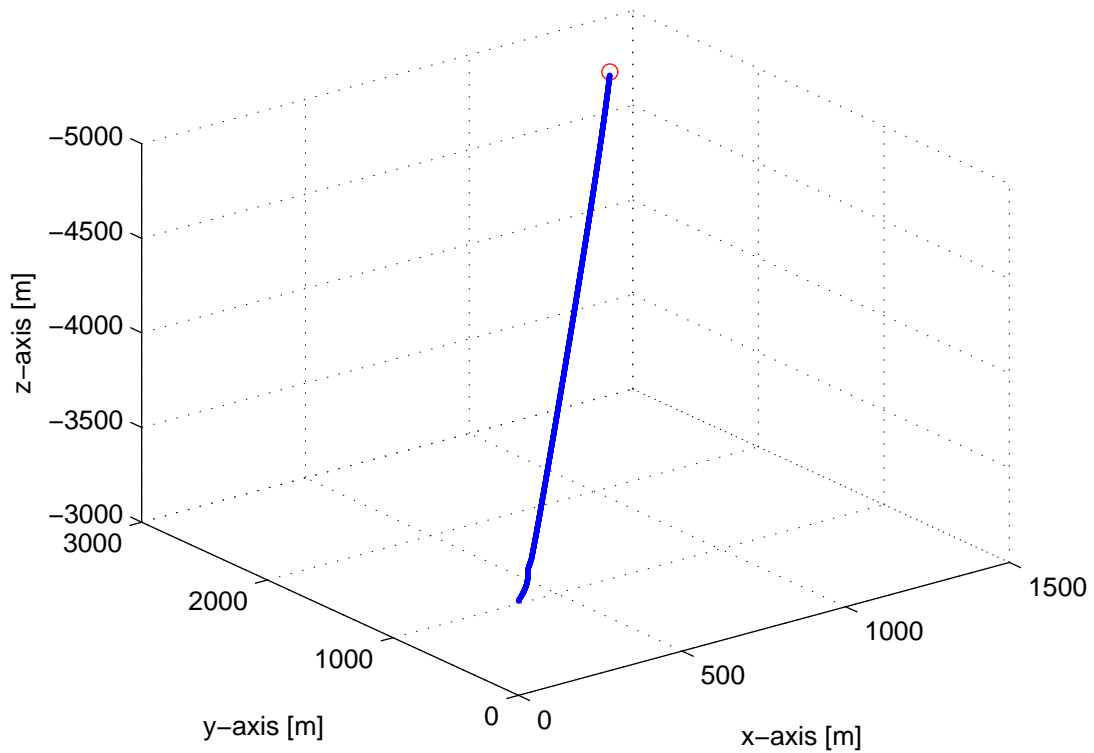


Figure 6.4: 3D visualisation of the missile trajectory (*in blue*) and interception of the stationary target (\circ).

Figure 6.4 displays a 3D visualisation of the missile trajectory. It can be seen from this figure that the robust control system proposed is capable of tracking the target and achieving interception in the presence of uncertainties and modeling errors introduced into the simulated system. In this section, the simulation considered the case where the target is stationary.

Chapter 7

Simulation - Non-Stationary

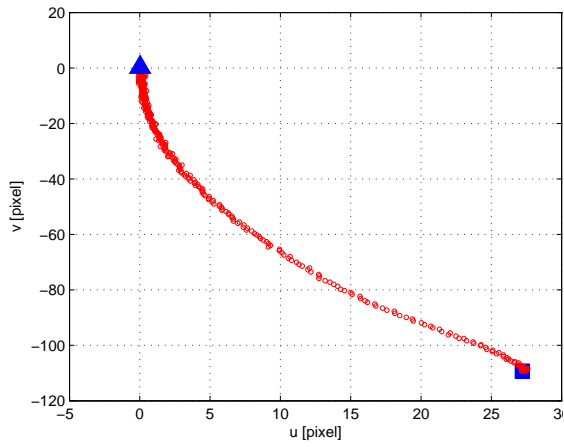
Target

The second simulation involved the evaluation of the proposed controller's performance in the presence of a moving target. The simulation parameters are identical to the first simulation with an addition of a moving target. The target's velocity is initialized as

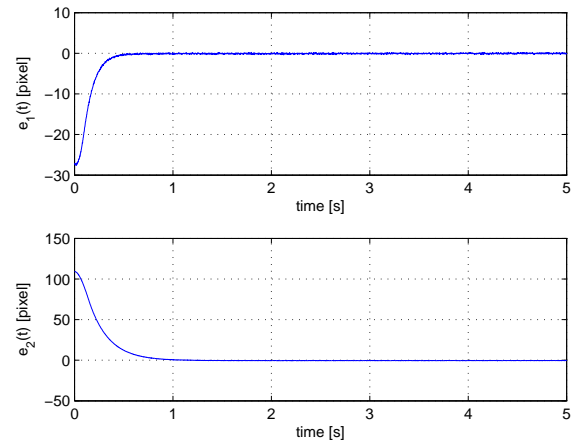
$$\dot{q}_t = [v_t \quad \omega_t] \quad (7.1)$$

$$v_t = [50 \quad 30 \quad 0]^T(m/s), \quad \omega_t = [0 \quad 0 \quad 0.05]^T(rad/s) \quad (7.2)$$

Figure 7.1 shows the tracking and error minimization capability of the proposed controller in the presence of a moving target. It can be seen that the controller drives the target toward the principal point and the error is reduced asymptotically.



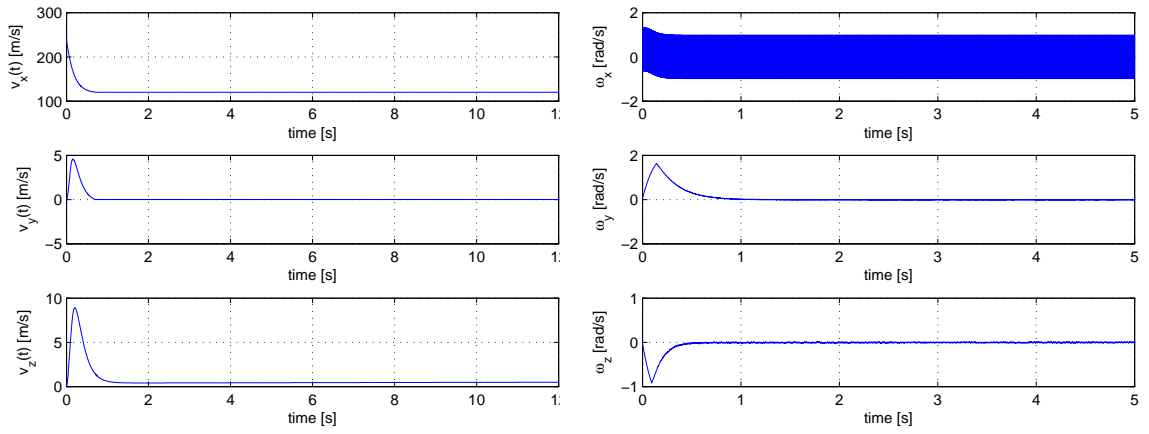
(a) Tracking



(b) Error in u and v

Figure 7.1: Tracking and error minimization performance is displayed for a non-stationary target.

The missile linear and angular velocities and the control input commands are plotted in Figures 7.2 and 7.3, respectively.



(a) Linear velocities of the missile

(b) Angular velocities of the missile

Figure 7.2: Linear and angular velocities of the missile along x, y , and z – axis measured with respect to the earth frame.

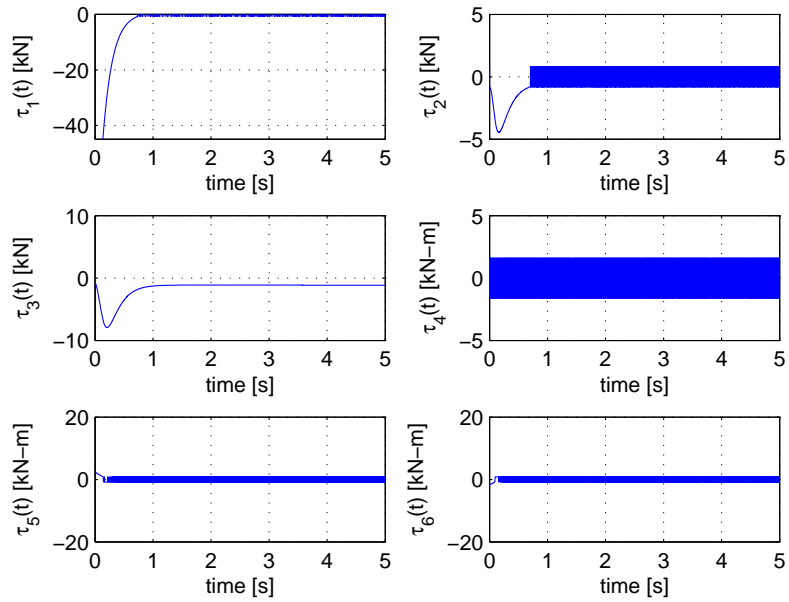


Figure 7.3: This plot shows the control input ($\tau(t)$) applied to the missile airframe during the simulation.

Finally, the trajectory of the missile in 3D Euclidean space is plotted in Figure 7.4. It was shown that the missile frame is also able to track a moving target and intercept it.

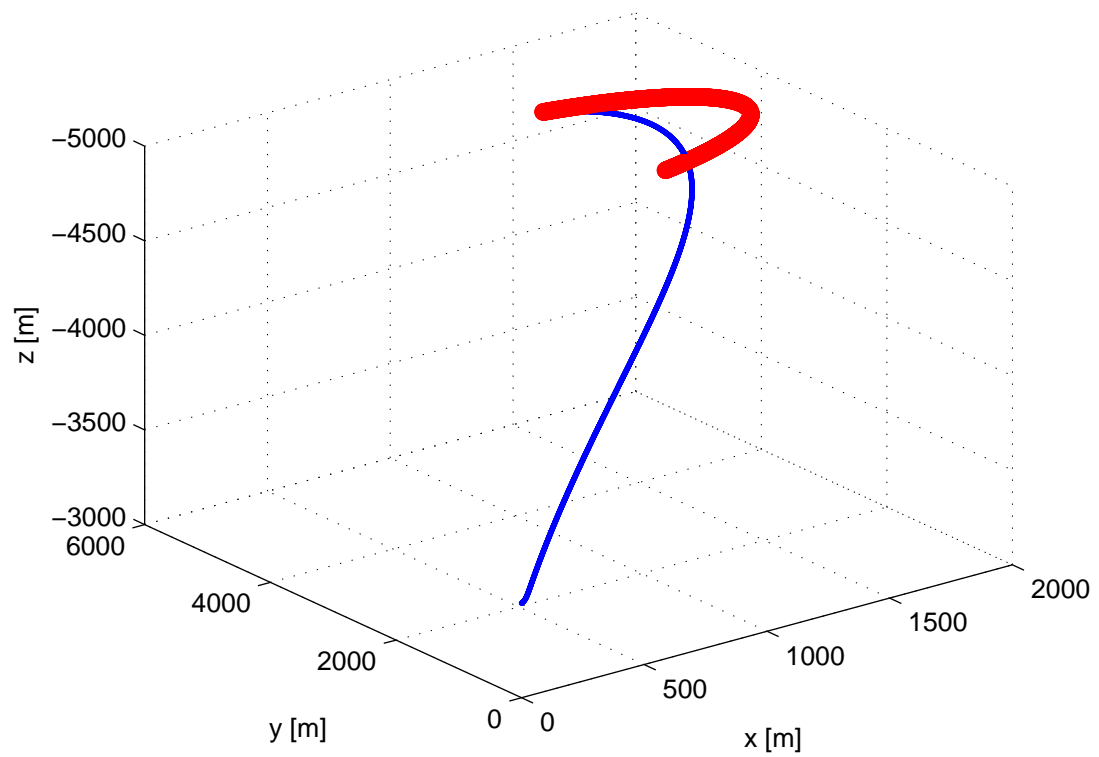


Figure 7.4: 3D visualization of the missile trajectory (*in blue*) and interception of the stationary target (\circ).

Chapter 8

Conclusion

A robust vision-based missile guidance law is presented for a missile equipped with a monocular camera system. The guidance law yields asymptotic target interception of a target in the presence of dynamic uncertainty and unknown target evasive maneuvers. The result is achieved by using an image-based visual servo control method, where the missile dynamics are combined with the target image kinematics of the monocular camera. The proposed control law is designed to be inexpensively implemented, requiring no online adaptive laws, NNs, or complex computations in the control loop. A Lyapunov-based stability analysis is used to prove that the proposed control law is capable of regulating the pixel coordinates of the target to the principle point. Once the target image coordinates are driven toward the principal point (optical axis), then the missile converges to a collision course. A numerical simulation is used to test the performance of the control law in the presence of stationary and non-stationary targets, where the plant model contains modeling errors and additive disturbances. The simulation results demonstrate that the proposed vision-based ro-

bust pursuit guidance law is capable of intercepting the target in both cases with zero miss distance.

Bibliography

Kuk-Whan Byun, Bong Wie, David Geller, and John Sunkel. Robust h (infinity) control design for the space station with structured parameter uncertainty. *Journal of guidance, control, and dynamics*, 14(6):1115–1122, 1991.

Kuk-Whan Byun, Bong Wie, David Geller, and John Sunkel. Robust h infinity control design for the space station with structured parameter uncertainty. In *Space Technology and Science*, volume 1, pages 1041–1046, 1992.

Francois Chaumette. Potential problems of stability and convergence in image-based and position-based visual servoing. In *The confluence of vision and control*, pages 66–78. Springer, 1998.

François Chaumette and Seth Hutchinson. Visual servo control. i. basic approaches. *Robotics & Automation Magazine, IEEE*, 13(4):82–90, 2006.

François Chaumette, Seth Hutchinson, et al. Visual servo control, part ii: Advanced approaches. *IEEE Robotics and Automation Magazine*, 14(1):109–118, 2007.

Chien Chern Cheah, Chao Liu, and Jean Jacques E Slotine. Adaptive jacobian vision based control for robots with uncertain depth information. *Automatica*, 46(7):1228–1233, 2010.

- Dongkyoung Chwa, Jin Young Choi, and Jin H Seo. Compensation of actuator dynamics in nonlinear missile control. *Control Systems Technology, IEEE Transactions on*, 12(4):620–626, 2004.
- C Copot, C Lazar, and A Burlacu. Predictive control of nonlinear visual servoing systems using image moments. *Control Theory & Applications, IET*, 6(10):1486–1496, 2012.
- Peter I Corke. A robotics toolbox for matlab. *Robotics & Automation Magazine, IEEE*, 3(1):24–32, 1996.
- Peter I Corke and Malcolm C Good. Dynamic effects in visual closed-loop systems. *Robotics and Automation, IEEE Transactions on*, 12(5):671–683, 1996.
- Peter I Corke and Seth A Hutchinson. A new partitioned approach to image-based visual servo control. *Robotics and Automation, IEEE Transactions on*, 17(4):507–515, 2001.
- Martin Corless and George Leitmann. Continuous state feedback guaranteeing uniform ultimate boundedness for uncertain dynamic systems. *Automatic Control, IEEE Transactions on*, 26(5):1139–1144, 1981.
- RA DeCarlo, SV Drakunov, and Xiaoqiu Li. A unifying characterization of robust sliding mode control: a lyapunov approach. *Journal of Dynamic Systems, Measurement, and Control*, 122:708, 2000.
- Koichiro Deguchi. Optimal motion control for image-based visual servoing by decoupling translation and rotation. In *Intelligent Robots and Systems, 1998. Pro-*

- ceedings.*, 1998 *IEEE/RSJ International Conference on*, volume 2, pages 705–711. IEEE, 1998.
- Warren E Dixon. Adaptive regulation of amplitude limited robot manipulators with uncertain kinematics and dynamics. *Automatic Control, IEEE Transactions on*, 52(3):488–493, 2007.
- Sergey Drakunov. Sliding mode control of the systems with uncertain direction of control vector. In *Decision and Control, 1993., Proceedings of the 32nd IEEE Conference on*, pages 2477–2478. IEEE, 1993.
- Sergey Drakunov and Vadim Utkin. Sliding mode observers. tutorial. In *Decision and Control, 1995., Proceedings of the 34th IEEE Conference on*, volume 4, pages 3376–3378. IEEE, 1995.
- Sergey Drakunov, Umit Ozguner, Peter Dix, and Behrouz Ashrafi. Abs control using optimum search via sliding modes. *Control Systems Technology, IEEE Transactions on*, 3(1):79–85, 1995.
- Sergey V Drakunov. Sliding-mode observers based on equivalent control method. In *Decision and Control, 1992., Proceedings of the 31st IEEE Conference on*, pages 2368–2369. IEEE, 1992.
- Keith Dupree, Nicholas R Gans, William MacKunis, and Warren E Dixon. Euclidean calculation of feature points of a rotating satellite: a daisy chaining approach. In *American Control Conference, 2007. ACC'07*, pages 3874–3879. IEEE, 2007.
- Paul G Grossimon, Enrique Barbieri, and Sergey Drakunov. Sliding mode control of

- an inverted pendulum. In *System Theory, 1996., Proceedings of the Twenty-Eighth Southeastern Symposium on*, pages 248–252. IEEE, 1996.
- Martin T Hagan and Howard B Demuth. Neural networks for control. In *American Control Conference, 1999. Proceedings of the 1999*, volume 3, pages 1642–1656. IEEE, 1999.
- Gregory D Hager, Wen-Chung Chang, and A Stephen Morse. Robot hand-eye coordination based on stereo vision. *Control Systems, IEEE*, 15(1):30–39, 1995.
- Tarek Hamel and Robert Mahony. Image based visual servo control for a class of aerial robotic systems. *Automatica*, 43(11):1975–1983, 2007.
- Dongchen Han and SN Balakrishnan. State-constrained agile missile control with adaptive-critic-based neural networks. *Control Systems Technology, IEEE Transactions on*, 10(4):481–489, 2002.
- Kurt Hornik, Maxwell Stinchcombe, and Halbert White. Multilayer feedforward networks are universal approximators. *Neural networks*, 2(5):359–366, 1989.
- Guoqiang Hu, William MacKunis, N Gans, Warren E Dixon, Jian Chen, Aman Behal, and D Dawson. Homography-based visual servo control with imperfect camera calibration. *Automatic Control, IEEE Transactions on*, 54(6):1318–1324, 2009.
- Seth Hutchinson, Gregory D Hager, and Peter I Corke. A tutorial on visual servo control. *Robotics and Automation, IEEE Transactions on*, 12(5):651–670, 1996.
- Hassan K Khalil. *Nonlinear systems*, volume 3. Prentice hall Upper Saddle River, 2002.

- H Jin Kim, David H Shim, and Shankar Sastry. Flying robots: modeling, control and decision making. In *Robotics and Automation, 2002. Proceedings. ICRA'02. IEEE International Conference on*, volume 1, pages 66–71. IEEE, 2002.
- Jack W Langelaan. State estimation for autonomous flight in cluttered environments. *Journal of guidance, control, and dynamics*, 30(5):1414–1426, 2007.
- Frank L Lewis. Neural network control of robot manipulators. *IEEE Expert*, 11(3):64–75, 1996.
- W Mackunis, N Gans, K Kaiser, and WE Dixon. Unified tracking and regulation visual servo control for wheeled mobile robots. In *Control Applications, 2007. CCA 2007. IEEE International Conference on*, pages 88–93. IEEE, 2007.
- W MacKunis, PM Patre, MK Kaiser, and WE Dixon. Asymptotic tracking for aircraft via robust and adaptive dynamic inversion methods. *Control Systems Technology, IEEE Transactions on*, 18(6):1448–1456, 2010a.
- W MacKunis, ZD Wilcox, MK Kaiser, and WE Dixon. Global adaptive output feedback tracking control of an unmanned aerial vehicle. *Control Systems Technology, IEEE Transactions on*, 18(6):1390–1397, 2010b.
- Ezio Malis, Francois Chaumette, and Sylvie Boudet. 21/2d visual servoing. *Robotics and Automation, IEEE Transactions on*, 15(2):238–250, 1999.
- Michael B McFarland and Anthony J Calise. Multilayer neural networks and adaptive nonlinear control of agile anti-air missiles. In *AIAA Guidance, Navigation and Control Conference*, pages 401–410, 1997.

- Michael B McFarland and Anthony J Calise. Adaptive nonlinear control of agile anti-air missiles using neural networks. *Control Systems Technology, IEEE Transactions on*, 8(5):749–756, 2000.
- Rafik Mebarki, Alexandre Krupa, and François Chaumette. 2-d ultrasound probe complete guidance by visual servoing using image moments. *Robotics, IEEE Transactions on*, 26(2):296–306, 2010.
- SS Mehta, William MacKunis, and JW Curtis. Adaptive vision-based missile guidance in the presence of evasive target maneuvers. In *World Congress, Proc. of 18th IFAC, Milano, Italy*, pages 5471–5476, 2011.
- SS Mehta, W MacKunis, EL Pasilio, and JW Curtis. Adaptive image-based visual servo control of an uncertain missile airframe. In *Guidance, Navigation and Control Conf.(GNC), Proc. of AIAA, Minneapolis, MN*, 2012a.
- SS Mehta, W MacKunis, S Subramanian, and CL Pasilio. Nonlinear control of hypersonic missiles for maximum target penetration. In *Guidance, Navigation and Control Conf.(GNC), Proc. of AIAA, Minneapolis, MN*, 2012b.
- Zoran Miljković, Marko Mitić, Mihailo Lazarević, and Bojan Babić. Neural network reinforcement learning for visual control of robot manipulators. *Expert Systems with Applications*, 2012.
- Yoshihiko Miyasato. Adaptive gain-scheduled h_j sub _{λ_j} /sub _{λ_j} control of linear parameter-varying systems with nonlinear components. In *American Control Conference, 2003. Proceedings of the 2003*, volume 1, pages 208–213. IEEE, 2003.

- Jongki Moon, Kiseok Kim, and Youdan Kim. Design of missile guidance law via variable structure control. *Journal of Guidance, Control, and Dynamics*, 24(4): 659–664, 2001.
- Norman S Nise. *CONTROL SYSTEMS ENGINEERING, (With CD)*. John Wiley & Sons, 2007.
- N Papanikolopoulos, PK Khosla, and T Kanada. Vision and control techniques for robotic visual tracking. In *Robotics and Automation, 1991. Proceedings., 1991 IEEE International Conference on*, pages 857–864. IEEE, 1991.
- Nikolaos P Papanikolopoulos, Pradeep K Khosla, and Takeo Kanade. Visual tracking of a moving target by a camera mounted on a robot: A combination of control and vision. *Robotics and Automation, IEEE Transactions on*, 9(1):14–35, 1993.
- Parag M Patre, William MacKunis, Kent Kaiser, and Warren E Dixon. Asymptotic tracking for uncertain dynamic systems via a multilayer neural network feedforward and rise feedback control structure. *Automatic Control, IEEE Transactions on*, 53(9):2180–2185, 2008.
- PM Patre, W MacKunis, C Makkar, and WE Dixon. Asymptotic tracking for systems with structured and unstructured uncertainties. In *Decision and Control, 2006 45th IEEE Conference on*, pages 441–446. IEEE, 2006.
- Zhihua Qu. *Robust control of nonlinear uncertain systems*. John Wiley & Sons, Inc., 1998.
- Ann E Rundell, Sergey V Drakunov, and Raymond A DeCarlo. A sliding mode

- observer and controller for stabilization of rotational motion of a vertical shaft magnetic bearing. *Control Systems Technology, IEEE Transactions on*, 4(5):598–608, 1996.
- Guna Seetharaman, Arun Lakhotia, and Erik Philip Blasch. Unmanned vehicles come of age: The darpa grand challenge. *Computer*, 39(12):26–29, 2006.
- Jean-Jacques E Slotine, Weiping Li, et al. *Applied nonlinear control*, volume 199. Prentice hall New Jersey, 1991.
- Omar Tahri, Youcef Mezouar, François Chaumette, and Peter Corke. Decoupled image-based visual servoing for cameras obeying the unified projection model. *Robotics, IEEE Transactions on*, 26(4):684–697, 2010.
- Vadim Utkin. Variable structure systems with sliding modes. *Automatic Control, IEEE Transactions on*, 22(2):212–222, 1977.
- Jacques Waldmann. Line-of-sight rate estimation and linearizing control of an imaging seeker in a tactical missile guided by proportional navigation. *Control Systems Technology, IEEE Transactions on*, 10(4):556–567, 2002.
- Qian Wang and Robert F Stengel. Robust nonlinear control of a hypersonic aircraft. *Journal of Guidance, Control, and Dynamics*, 23(4):577–585, 2000.
- Bong Wie. *Space vehicle dynamics and control*. Aiaa, 1998.
- SW Wijesoma, DFH Wolfe, and RJ Richards. Eye-to-hand coordination for vision-guided robot control applications. *The International Journal of Robotics Research*, 12(1):65–78, 1993.

- Zachary D Wilcox, William MacKunis, S Bhat, R Lind, and WE Dixon. Robust nonlinear control of a hypersonic aircraft in the presence of aerothermoelastic effects. In *American Control Conference, 2009. ACC'09.*, pages 2533–2538. IEEE, 2009.
- Haojian Xu, Maj D Mirmirani, and Petros A Ioannou. Adaptive sliding mode control design for a hypersonic flight vehicle. *Journal of Guidance, Control, and Dynamics*, 27(5):829–838, 2004.
- Rafael Yanushevsky. *Modern missile guidance*. CRC Press, 2007.
- K David Young, Vadim I Utkin, and Umit Ozguner. A control engineer’s guide to sliding mode control. In *Variable Structure Systems, 1996. VSS'96. Proceedings., 1996 IEEE International Workshop on*, pages 1–14. IEEE, 1996.
- R Zaeim, MA Nekoui, and A Zaeim. Integration of imaging seeker control in a visually guided missile. In *Control and Automation (ICCA), 2010 8th IEEE International Conference on*, pages 46–51. IEEE, 2010.
- Stanislaw H Zak. *Systems and control*, volume 388. Oxford University Press New York, 2003.
- Hu Zhubing, Zhou Dezhi, Han Wenlong, et al. Robust nonlinear control of a hypersonic aircraft based on sliding mode control. *Procedia Engineering*, 29:837–842, 2012.
- Qun Zong, Yuehui Ji, Fanlin Zeng, and Helong Liu. Output feedback back-stepping control for a generic hypersonic vehicle via small-gain theorem. *Aerospace Science and Technology*, 2011.